Open access • Posted Content • DOI:10.1101/2020.04.07.029181

Crystal structure of full-length cytotoxic necrotizing factor CNFY reveals molecular building blocks for intoxication — Source link

Paweena Chaoprasid, Peer Lukat, Sabrina Mühlen, Thomas Heidler ...+10 more authors

Institutions: University of Münster

Published on: 21 Sep 2020 - bioRxiv (Cold Spring Harbor Laboratory)

Crystal structure of full-length cytotoxic necrotizing factor CNF_Y reveals molecular building blocks for intoxication

Paweena Chaoprasid[1,2*], Peer Lukat[3*], Sabrina Mühlen[1,2,4*], Thomas Heidler[5], Emerich-Mihai Gazdag[3], Shuangshuang Dong[3], Wenjie Bi[6], Christian Rüter[1], Marco Kirchenwitz[7], Anika Steffen[7], Lothar Jänsch[6,8], Theresia E. B. Stradal[7,8], Petra Dersch[1,2,4,9#] & Wulf Blankenfeldt[3,10#]

[1]Institute of Infectiology, Center for Molecular Biology of Inflammation (ZMBE), University of Münster, Von-Esmarch-Straße 56, 48149 Münster, Germany

[2]Molecular Infection Biology, Helmholtz Centre for Infection Research, Inhoffenstr. 7, 38124 Braunschweig, Germany

[3]Structure and Function of Proteins, Helmholtz Centre for Infection Research, Inhoffenstr. 7, 38124 Braunschweig, Germany

[4]Deutsches Zentrum für Infektionsforschung, Inhoffenstr. 7, 38124 Braunschweig

[5]Molecular Structural Biology, Helmholtz Centre for Infection Research, Inhoffenstr. 7, 38124 Braunschweig, Germany

[6]Cellular Proteomics, Helmholtz Centre for Infection Research, Inhoffenstr. 7, 38124 Braunschweig, Germany

[7]Cell Biology, Helmholtz Centre for Infection Research, Inhoffenstr. 7, 38124 Braunschweig, Germany

[8]Institute of Zoology, Technische Universität Braunschweig, Spielmannstr. 7, 38106 Braunschweig, Germany

[9]Institute of Microbiology, Technische Universität Braunschweig, Spielmannstr. 7, 38106 Braunschweig, Germany

[10]Institute for Biochemistry, Biotechnology and Bioinformatics, Technische Universität Braunschweig, Spielmannstr. 7, 38106 Braunschweig, Germany

*equal contribution
#corresponding authors

Running title: Structure-function analysis of CNF_Y toxin

Abstract

Cytotoxic necrotizing factors (CNFs) are bacterial single-chain exotoxins that modulate cytokinetic/oncogenic and inflammatory processes through activation of host cell Rho GTPases. To achieve this, they are secreted, bind surface receptors to induce endocytosis and translocate a catalytic unit into the cytosol to intoxicate host cells. A three-dimensional structure that provides insight into the underlying mechanisms is still lacking. Here, we determined the crystal structure of full-length *Yersinia pseudotuberculosis* CNF_Y. CNF_Y consists of five domains (D1-D5), and by integrating structural and functional data we demonstrate that D1-3 act as export and translocation module for the catalytic unit (D4-5) or fused β-lactamase reporter proteins. We further found that domain D4, which possesses structural similarity to ADP-ribosyl transferases, but had no equivalent catalytic activity, changed its position to interact extensively with D5 in the crystal structure of the free D4-5 fragment. This liberates D5 from a semi-blocked conformation in full-length CNF_Y, leading to higher deamidation activity. Finally, sequence comparisons identified the CNF translocation module in many uncharacterized bacterial proteins, suggesting its usability as a universal drug delivery tool.

Introduction

Amongst the plethora of traits developed by pathogenic bacteria to establish infections, toxins play the most prominent role, since they are responsible for the majority of clinical symptoms (Popoff, 2005). Many bacterial exotoxins are key virulence factors that target different functions of host cells to break barriers, improve access to nutrients, defeat immune responses and promote bacterial dissemination within and among hosts.

The cytotoxic necrotizing factors (CNFs) belong to a class of bacterial exotoxins that deamidate a glutamine (Q61 or Q63) in the active site (switch II region) of host cell proteins belonging to the small Rho GTPase family, i.e. RhoA, Rac1 and Cdc42 (Flatau *et al*, 1997; Schmidt *et al*, 1997; Knust & Schmidt, 2010). This locks these key regulators in their active state, causing a multitude of downstream effects that are most readily observed as alterations of the actin cytoskeleton or perturbations of other cellular processes including phagocytosis, cell proliferation (multinucleation), reactive oxygen species production, and the release of anti-apoptotic and pro-inflammatory factors (Fabbri *et al*, 2013; Hodge & Ridley, 2016; Ho *et al*, 2018). The consequences of these effects are changes of innate immune responses and tissue damage, leading to the development of acute disease symptoms (Knust & Schmidt, 2010; Schweer *et al*, 2013; Diabate *et al*, 2015; Cavaillon, 2018; Heine *et al*, 2018).

CNFs are found in several pathogenic bacteria, predominantly in pathogenic *Escherichia coli*, but also in *Yersinia pseudotuberculosis*, *Shigella* species, *Salmonella enterica,* as well as in *Moritella viscosa* and *Photobacterium damselae*, pathogens of economically important fish (Fig EV1) (Morgan *et al*, 2019). In addition, CNFs show local homology to other toxins such as the dermonecrotizing toxin DNT of *Bordetella pertussis* and the PMT toxin of *Pasteurella multocida* (Walker & Weiss, 1994), indicating that these proteins consist of common structural building blocks that have been interchanged in the course of evolution.

CNF1, the most thoroughly investigated representative of the CNF family, is a major virulence factor in uropathogenic *E. coli* (UPEC) strains, which live in the intestine and enter the urinary tract via the urethra (Boquet, 2001; Knust & Schmidt, 2010; Ho *et al*, 2018).

CNF1-containing strains exhibit a higher viability, have a higher potential to colonize the urinary tract, affect the function of immune cells and increase the inflammation rate (Falzano *et al*, 1993; Fournout *et al*, 2000; Rippere-Lampe *et al*, 2001). CNF1 was also identified in some intestinal and extraintestinal *E. coli* (ExPEC) where it was found to increase bacterial invasion into endothelial cells (Khan *et al*, 2002) and to promote malignant tumor conversion and intestinal cell invasiveness (Zhang *et al*, 2018; Fabbri *et al*, 2019). Similarly, the homologous toxin CNF_Y, which shares 65% identity with *E. coli* CNF1, is crucial for the pathogenicity of *Y. pseudotuberculosis*, which causes food-borne and zoonotic enteric infections that manifest themselves as enteritis, mesenterial lymphadenitis and more rarely, in sequelae such as reactive arthritis (Koornhof *et al*, 1999a; Smego *et al*, 1999; Heine *et al*, 2018). The importance of CNF_Y is emphasized by the fact that a knock-out mutation of the *cnfY* gene leads to avirulence, allowing bacteria to become persistent in mice (Heine *et al*, 2018). Recent studies demonstrated that Rho GTPase activation by CNF_Y enhances the translocation of *Yersinia* outer proteins (Yops) into neutrophils and macrophages via a type III secretion system (T3SS). This blocks phagocytosis, triggers immune cell death and contributes to massive tissue damage by induction of pro-inflammatory responses and necrosis (Schweer *et al*, 2013; Wolters *et al*, 2013).

CNFs may also hold promise for treatment of neurological disorders and cancer (Maroccia *et al*, 2018). For example, CNF1 injection into brains of mice enhanced neuro-transmission and synaptic plasticity, leading to improved learning and memory (Diana *et al*, 2007). Moreover, CNF1 was able to rescue wildtype-like mitochondrial morphology in fibro-blasts derived from patients with myoclonic epilepsy, and it reduced tumor growth (Vannini *et al*, 2016; Fabbri *et al*, 2018). As CNFs efficiently intoxicate a broad range of host cells, transport modules of the toxin may also be useful for drug delivery (Haywood *et al*, 2018). To exploit and further develop this tool, detailed knowledge of the molecular mechanisms underlying CNF secretion, translocation and activity is required. However, little is known about the global structure and the individual functional units of CNFs and so far, only the structure of the catalytic domain of CNF1 has been determined (Buetow *et al*, 2002).

Structure-function analysis of CNF_Y

At the sequence level, CNF-type toxins of different species share at least 55% overall identity (Fig EV1), indicating similar structures and conserved modes-of-action, although they show differential preferences with respect to the targeted Rho GTPase and interact with different host cell receptors (Hoffmann *et al*, 2004; Blumenthal *et al*, 2007). CNF1 uses two cellular receptors to enter host cells, the 37-kDa laminin receptor precursor p37LRP, which is recognized by sequences located within the N-terminus of the toxin, and the Lutheran adhesion glycoprotein/basal cell adhesion molecule (Lu/BCAM), which interacts with motifs in the C-terminal half (Fabbri *et al*, 1999; Chung *et al*, 2003; Kim *et al*, 2005; McNichol *et al*, 2007; Piteau *et al*, 2014; Reppin *et al*, 2017). The receptor of the N-terminal part of CNF_Y is still unknown, but it has been shown that binding of CNF1 to host cells has no effect on CNF_Y uptake (Blumenthal *et al*, 2007), suggesting that both toxins use different host cell factors to enter host cells. This has also been corroborated in a recent study that identified glycosaminoglycans as interaction partners of C-terminal fragments of CNF_Y (Kowarschik *et al*, 2020). The CNFs are taken up into endosomes and their release into the host cytoplasm requires two hydrophobic sequence motifs within the N-terminal half of the toxin that have been predicted to form α-helices. These helices are separated by a loop containing an acidic patch of four conserved acidic amino acids, and they are believed to insert into the endosomal membrane upon charge neutralization of the patch in the course of endosome acidification (Pei *et al*, 2001). An unidentified protease then cleaves CNF (i.e. CNF1 between residues 532 and 544), and the C-terminal fragment including the catalytic domain (residues 720-1014) is released into the cytosol of the host cell to mediate the cellular effects of the toxin (Pei *et al*, 2001; Knust *et al*, 2009).

In this study, we resolved the crystal structure of the full-length *Y. pseudotuberculosis* CNF_Y protein, necessary to achieve an understanding of its transport and functional mechanisms and its potential therapeutic use. The CNF_Y structure revealed a complex set-up of five individual building blocks and allowed us to obtain detailed information about the minimal secretion and translocation domain required to transport the catalytic domain or a fused cargo protein into the host cell cytosol, which could be exploited for drug delivery.

Results

CNF_Y contains five structural building blocks

Recombinant full-length CNF_Y was produced in *E. coli* (Appendix Fig S1) and crystallized in space group $I2_12_12_1$. These crystals diffracted to 2.7 Å and contained one CNF_Y molecule in the asymmetric unit. Since no suitable search model for molecular replacement was available and crystallization of full-length seleno-*L*-methionine-labelled protein failed, we also crystallized different fragments of CNF_Y: (i) one containing only the deamidase domain (residues 720-1014), (ii) another consisting of the subunit which is likely released into the cytosol (residues 526-1014) based on the homology to *E. coli* CNF1 (Hoffmann *et al*, 2004; Blumenthal *et al*, 2007), and (iii) a third fragment including the complete N-terminal portion with parts of the released subunit (residues 1-704) (Appendix Fig S1). A detailed description of structure determination by Se-SAD and molecular replacement is given in the Materials and Methods section and an overview over data collection and refinement statistics as well as the respective Protein Data Bank (Berman *et al*, 2000) deposition codes is provided in Table EV1.

CNF_Y adopts a compact, modular structure of five structural building blocks (D1-D5) with approximate dimensions of 115*73*65 Å (Fig 1A-C). All residues of the protein could be traced in the structure of the holo-protein with the exception of residues N430-K431, S550-L553 and P701-L717. The unresolved amino acids resided in surface loops, indicating intrinsic flexibility. Analysis with PiSQRD (Aleksiev *et al*, 2009) assigns domain boundaries to residues 1-22/135-424 (D1), 23-134 (D2), 425-529 (D3), 530-700 (D4) and 718-1014 (D5, deamidase domain). The compact arrangement of D1-D5 in the full-length structure of CNF_Y prompted us to investigate the interactions between the five individual domains of CNF_Y in more detail. Analysis with PISA (Krissinel & Henrick, 2007) reveals large hydrophobic interfaces between D1 and D2 (interface area 870 $Å^2$) as well as between D3 and D4 (750 $Å^2$) (Appendix Tab S1). The C-terminal domain D5 interacts mainly with D3 (610 $Å^2$), which, as a consequence, partially blocks the entrance to the catalytic site. D5

interacts only weakly with D4 (380 $Å^2$), which itself establishes an extensive interface with D1 (1390 $Å^2$) (Fig 1C).

The crystal structure of the fragment comprising residues 1-704 (D1-D4) is fully superimposable with the respective residues of the holo-protein. The isolated D4-D5 fragment, on the other hand, showed a different orientation of the two domains with respect to the full-length protein and was thus included into the following more detailed structure-functional analysis together with full-length CNF_Y.

Structural analysis and structure-guided mutagenesis provide insight into the function of the structural building blocks of CNF_Y

In order to gain insights into the biological function of the individual building blocks, we performed a detailed structural analysis of the full-length CNF_Y (D1-D5) and constructed truncated, mutated and marker-tagged versions of CNF_Y to investigate their secretion, translocation and enzymatic activity in human epithelial cells. The truncations were designed to interrupt the protein within linker regions between the individual domains (Fig 2A). CNF_Y variants were produced in *Y. pseudotuberculosis* or as recombinant proteins from *E. coli* (Fig 2B, Appendix Fig S1). Their enzymatic activity was tested with bacterial extracts or purified proteins by assessing their ability to deamidate RhoA in intact HEp-2 cells and host cell extracts, and by assessing the induction of actin rearrangements and the inhibition of cell division (formation of multinuclear cells) (Fig 3). The ability to bind to host cells was tested with 3xFlag-tagged versions of the CNF_Y derivatives (Figs 2D), and their capacity to reach late endosomes was measured with CNF_Y-GFP fusion variants (Fig 4). CNF_Y export from the bacterial cell and cytosolic translocation of the CNF_Y activity domain were detected with CNF_Y-β-lactamase (TEM) constructs (Figs 2C, 3A). Secretion of the CNF_Y-TEM derivatives was analyzed by incubation of bacterial culture supernatants with nitrocefin, a chromogenic cephalosporin substrate used to detect β-lactamases. Translocation of the CNF_Y-TEM fusion proteins was detected by staining the cytosol of host cells with the FRET substrate CCF4-AM, which contains the coumarin- and fluorescein-

conjugated β-lactam cephalosporin and is green fluorescent (excitation at 409 nm, emission at 530 nm). Cleavage of the β-lactam ring shifts the fluorescence of the compound to blue (emission at 450 nm) and thus indicates the presence of TEM β-lactamase in the cytosol.

For validation, we first tested marker-tagged full-length wildtype CNF_Y (CNF_Y 1-1014) and a mutant derivative, namely CNF_Y C866S. This substitution inactivated the deamidase activity when introduced into *E. coli* CNF1 (Hoffmann *et al*, 2004). The marker-tagged versions of the full-length CNF_Y wildtype protein were efficiently produced (Fig. 2B), secreted (Fig 2C), and internalized into host cells (Fig 2D). Inside cells they were targeted to the late endosome (Fig 4) and translocated into the host cell cytosol (Fig 3A) to deamidate RhoA (Fig 3B) and induce formation of stress fibers or polynucleation in cultured cells (Fig 3C). In contrast, all CNF_Y C866S derivatives were found to abrogate the RhoA deamidation and induction of multinucleated cells, whereas other properties were not affected (Fig 2B-D, 3). Together, this demonstrates the suitability of the employed test systems.

Domain D1 is a major component of the translocation apparatus in CNFs

The crystal structure of CNF_Y revealed that domain D1 consists of separate areas covering residues 1-22 and 135-424, which together form a bundle of α-helices flanked by a four-stranded anti-parallel β-sheet that is covered with three α-helices from the other side (Fig 1B, Fig EV2). Sequences within domain D1 have previously been shown to contain elements that are required for translocation of the catalytic fragment of *E. coli* CNF1 (Pei *et al*, 2001; Knust *et al*, 2009), suggesting that this domain is a major component of the translocation machinery of CNFs.

Although domain D1 of CNF_Y is, due to its overall α-helical character, reminiscent of the translocation domain of other toxins such as diphtheria toxin (DT), searches with DALI (Holm & Rosenström, 2010) detected no significant structural homology to these proteins. Instead, it identified only the segment containing the four-stranded anti-parallel β-sheet (residues 152-343) as being somewhat similar to a fragment of the translocation domain of nigritoxin, a toxin of crustaceans and insects (PDB entry 5M41; 177 residues aligned, rmsd

3.8 Å, 11% sequence identity) (Fig 5A) (Labreuche *et al*, 2017). However, the translocation domain of nigritoxin is significantly smaller than the D1 domain of CNF_Y and does not contain hydrophobic sequence motifs that have previously been predicted to be essential for translocation in CNFs and other toxins (Pei *et al*, 2001; Orrell *et al*, 2017), hinting at distinct translocation mechanisms.

To gain further insight into the function of D1, we constructed marker-tagged CNF_Y derivatives different deletions within the domain (Δ39-134, Δ134-426, Δ39-426; Fig 2A). The CNF_Y Δ134-426 derivative was less efficiently produced and inactive (i.e. it did not deamidate RhoA in host cell extracts, Fig 2B and 3B), indicating that it is improperly folded and less stable. However, the CNF_Y Δ39-134 and CNF_Y Δ39-426 proteins were well expressed and enzymatically active, yet, they failed to be secreted (Fig 2B-C), and consequently unable to trigger RhoA activation when added to host cells (Fig 3B). On the other hand, a C-terminally truncated CNF_Y protein containing the entire domain D1 (1-443) was secreted efficiently (Fig 2C), corroborating that this segment is necessary and sufficient for CNF_Y to exit the bacterial cell.

Use of CNF_Y-TEM derivatives further revealed that all deletions of or within domain D1 abolished translocation of the active domain into the host cell cytoplasm when added to host cells (Fig 3A), although CNF_Y Δ39-134 and CNF_Y Δ39-426 derivatives were still able to bind and enter cells (Fig 2D), and associate with the late endosome (Fig 4). This demonstrated that domain D1 is an important component of the translocation machinery but not essential for host cell binding and endocytosis.

For *E. coli* CNF1, two hydrophobic α-helices have been predicted between residues 350-372 and 387-412, which are believed to insert into the endosomal membrane after charge neutralization of a conserved acidic patch in the connecting loop (D373, D379, E382 and E383) (Pei *et al*, 2001). However, the respective segments do not fold into the predicted α-helices in CNF_Y but adopt mostly loop-like structures with a helical part at their C-terminus (Fig 1B, Fig EV2), which may be a consequence of the neutral pH at which CNF_Y has been crystallized here. In line with previous work on *E. coli* CNF1, site-directed mutagenesis of

the acidic residues E382 and E383 in the acidic patch to lysines did not abolish the enzymatic activity of the toxin derivative when added to cell lysates (Appendix Fig. S2). The CNF_Y E382K/E383K variant was still secreted and able to enter cells but failed to activate RhoA and induce multinucleation (Appendix Fig S2). This supported previous assumptions that acidic residues in the connecting loop are important for translocation (Pei *et al*, 2001).

Importantly, domain D1 alone does not seem to be sufficient for the translocation process, as the C-terminally truncated derivative CNF_Y 1-443, consisting of domains D1-D2, was unable to translocate the β-lactamase TEM cargo protein into the cytosol, deamidate RhoA in host cells and induce multinucleation (Fig 3), despite the fact that it was internalized and reached late endosomes (Fig 4). This indicated that the translocation machinery of CNFs requires additional components for functionality.

Domain D2 is a receptor binding domain of CNFs

Unlike the N-terminal α-helix (residues 5-18), which is an integral part of the helical bundle that dominates domain D1, residues 23-134 seem to establish a separate structural building block (domain D2) that protrudes from the mostly α-helical subunit, potentially suggesting its insertion during evolution (Fig 1B). It consists of a three-stranded anti-parallel β-sheet flanked by α-helices at the side facing D1 and by several surface-exposed loops at the other. One solvent-exposed loop contains residues 53-75, a segment that has previously been implicated in host cell binding of *E. coli* CNF1 to receptor p37LRP/LR67 (Fig 1B, Fig EV2) (Fabbri *et al*, 1999; Chung *et al*, 2003; Kim *et al*, 2005). It is hence conceivable that this domain represents the N-terminal receptor binding domain of CNFs. The solvent-exposed loop interacts with residues 112 to 116 at the surface of D2, such that these segments together may establish a receptor-binding interface of the CNFs (Fig EV2). There are ten amino acid changes between CNF1 and CNF_Y within these regions (Fig EV1), which may account for the distinct receptor specificity of both toxins (Blumenthal *et al*, 2007).

As outlined above, host cell binding and colocalization studies with truncated CNF_Y derivatives showed that the D1-2 (1-443) fragment was able to bind host cells (Fig 2D) and

reached the late endosomes (Fig 4), indicating that this truncated version of CNF_Y indeed includes a cell receptor binding site similar to CNF1 (Fabbri *et al*, 1999; Chung *et al*, 2003; Kim *et al*, 2005). However, this also demonstrates that CNF_Y, unlike previous work with CNF1 suggests (Piteau *et al*, 2014; Reppin *et al*, 2017), does not require a second recognition site in the C-terminal region to enter host cells.

Domain D3 is an essential part of the translocation apparatus of CNFs:

The third domain, D3 (residues 425-529), is reminiscent of an incomplete β-barrel, containing six anti-parallel strands in CNF_Y. No homologous structures could be discovered with DALI. Because a fragment consisting only of domains D1-2 (CNF_Y 1-443) was not able to translocate the fused TEM-β-lactamase into the host cell cytosol whereas the D1-3 fragment (CNF_Y 1-526) was (Fig 3A), D3 is obviously essential for intoxication. D1-3 translocated TEM-β-lactamase with the same efficiency as full-length CNF_Y (Appendix Fig. S3), and although it is unclear whether β-lactamase was released from D1-3 or only exposed on the cytosolic side from the endosomal membrane, these experiments clearly demonstrated that the translocation apparatus of CNFs consists of the three domains D1-3. The importance of D3 is also highlighted by the fact that (i) the N-terminus of *Pasteurella multocida* exotoxin PMT possesses high homology to D1-3 of CNF_Y, whereby cargo delivery includes proteolytic cleavage downstream of the prospective D3 domain, and (ii) the finding that a hybrid toxin consisting of this N-terminal fragment (residues 1-505) of PMT and the ADP-ribosylating domain of DT was able to intoxicate cells (Bergmann *et al*, 2013; Clemons *et al*, 2018).

The cleavage site between D3 and D4 is partially shielded in full-length CNF_Y

The imperfect β-barrel domain D3 and the following domain D4 are connected via a linker that is partially shielded by the C-terminal deamidase domain D5 in the structure of full-length CNF_Y (Fig 1C). In CNF1, this linker is cleaved between residues 532-544 to release the D4-5 subunit into the host cell cytosol (Knust *et al*, 2009), suggesting that the respective

segment must become solvent-exposed in the course of host cell intoxication to be accessible to proteases. As outlined below, this likely is linked to unfolding during translocation of the D4-5 segment into the cytosol of the host cell.

In order to identify amino acids that are important for the cleavage step, we introduced mutations within this linker. All recombinant mutant proteins were able to bind to host cells and deamidate RhoA in cell lysates, indicating proper folding and full activity (Fig 6). Interestingly, the CNF_Y I535L/P536A/V537G mutant with changes in the N-terminal part of the linker (CNF_Y mut1) promoted translocation into the host cell cytoplasm and was able to deamidate RhoA when added to host cells (Fig 6). However, this was not the case for the CNF_Y variant I535L/P536A/V537G/F539L/D541A/K542A (Fig 6), suggesting that this variant is unable to escape the endosome. In summary, this indicated that amino acids important for proper processing are located at the C-terminal end of the linker.

Domain D4 has structural similarity to ADP-ribosyl transferases

Sequence analysis places the fourth domain D4 (residues 530-700) into the DUF4765 family, a building block that is also found in a number of other uncharacterized bacterial proteins (Fig EV3A). Surprisingly, structure similarity searches reveal distant but significant homology to ADP-ribosyl transferase (ART) domains (Appendix Tab S2), which are wide-spread in protein toxins (Fieldhouse & Merrill, 2008). This similarity is exemplified by two examples (*Clostridium perfringens* iota toxin, PDB entry 4H03 (Tsurumura *et al*, 2013); *Pseudomonas aeruginosa* ExoA, PDB entry 2ZIT (Jørgensen *et al*, 2008)) shown in Fig 5B and Fig EV3.

In order to gain further insight into the function of domain D4, which is translocated and released together with the catalytic domain, we analyzed two mutant variants harboring internal deletions of amino acids 527-719 or 527-699. However, both variants did not deamidate RhoA in host cell lysates, indicating that these mutant proteins failed to fold properly (Appendix Fig S4). Since structure similarity searches revealed distant homology to the ADP-ribosyltransferase (ART) domains, we hypothesized that CNFs may possess a

second, previously unrecognized enzymatic function encoded in D4. The active sites of ARTs fall into two groups, the RSE- for a conserved arginine-serine-glutamate active site motif and the HYE-ARTs for histidine-tyrosine-glutamate (Cohen & Chang, 2018). The ART-like domain D4 contains arginine, glutamate and histidine at the respective positions instead (R599, E639, H676), which could, in principle, support similar chemistry and are, with the exception of the CNF-specific H676, highly conserved in other DUF4765-containing proteins (Fig EV3A). However, exchange of CNF_Y E639, which is in the comparable position of the conserved glutamate of bacterial ARTs, to alanine or glutamine had no effect on CNF_Y function (Appendix Fig S5). Moreover, we could not detect binding of the ART cosubstrate NAD^+ to a CNF_Y fragment consisting of domains D4-5 in microscalar thermophoresis titration experiments. The inability to bind NAD^+ may be a consequence of the altered geometry of the potential NAD^+ binding site of D4, which leads to a shallower hypothetical NAD^+ binding site and to clashes when NAD^+ is superimposed from the two examples mentioned above (Fig EV3B).

Domain D5 is highly similar to the deamidase domain of CNF1

The C-terminal catalytic deamidase domain D5 is linked to D4 via the unstructured residues P701-L717 (Fig 1B). These belong to the postulated binding epitope for the Lu/BCAM host receptor of CNF1 (Piteau *et al*, 2014), and their flexibility may be a requirement for receptor binding by the toxin.

The D5 domain is very similar to the respective domain of *E. coli* CNF1 (PDB entry 1HQ0 (Buetow *et al*, 2001); 1.8 Å rmsd over 295 residues, 59% sequence identity), featuring a central β-sandwich with shielding α-helices on both sides (Figs 1B and 5C). The active site employs the conserved cysteine/histidine couple C866/H881 (Hoffmann *et al*, 2004), which lies in a crevice on the surface of the domain and deamidates a conserved glutamine in the switch-II region of the targeted Rho GTPases. In agreement, only the full length CNF_Y protein was able to activate the Rho GTPase RhoA (Fig 3B), resulting in the induction of polynucleation in living cells (Fig 3C), whereas all protein variants with deletions of the C-

terminal domain D5 eliminated toxicity (Figs 3B-C). This is consistent with studies showing that the C-terminal 300 amino acids (709-1014) of the related *E. coli* CNF1 protein are important for its activity (Koornhof *et al*, 1999b; Zhang *et al*, 2018; Fabbri *et al*, 2019). Neither the deletion nor site-directed mutagenesis of the catalytic domain affected secretion, host-cell binding, or protein translocation (Figs 2B-C and 3A), indicating that the sole role of the C-terminal domain is the targeting and modification of Rho GTPases.

While the crevice is nearly identical between CNF_Y and CNF1, differences exist between two loops at the periphery of the active site, namely residues 961-970 and residues 996-1004 (Fig 5C, Fig EV1). It is not clear if these deviations are sufficient to explain the slightly altered preferences for various Rho GTPases that have been described for both CNFs (Hoffmann *et al*, 2004; Schweer *et al*, 2013), but amino acids in one of these loops (residues 961-970) has previously been implicated in substrate recognition of CNF_Y and CNF1 (Hoffmann *et al*, 2007). Interestingly, a similar deamidation domain is also found in *Burkholderia* lethal factor 1 (BLF1), despite extremely low sequence similarity (Fig 5C; PDB entry 3TU8; (Cruz-Migoni *et al*, 2011); 3.5 Å rmsd over 169 residues, 7% sequence identity). BLF1 is a single-domain toxin that deamidates a glutamine residue in translation initiation factor eIF4A. In addition, several other toxins including e.g. *Bordetella pertussis* dermonecrotizing toxin DNT are predicted to contain similar deamidase domains (Ho *et al*, 2018).

The D4-5 fragment of CNF_Y contains a receptor binding site sufficient for endosomal uptake

We further characterized the properties of the recombinant D4-5 domains (residues 526-1014), which together constitute the C-terminal fragment that is translocated into the host cell cytoplasm after cleavage of CNF_Y (Fig EV4). Although catalytically active when added to host cell extracts, D4-5 is unable to deamidate RhoA when added to host cells (Fig EV4E-D). This suggested that it was either not taken up into the host cell or unable to escape the endosome to reach the cytoplasm. Cell binding assays demonstrated, however, that the D4-5 fragment (CNF_Y 526-1014), similar to D1-3 (CNF_Y 1-526), specifically interacts with

host cells (Fig 2D, Fig EV4C and S6). A parallel analysis of D3-5 (CNF_Y 426-1014), also missing the N-terminal receptor binding domain, confirmed these results (Fig EV4C). This indicated the presence of a second host cell binding site in the C-terminal region, which is strongly supported by the fact that N-terminal deletions missing parts of D1-2 (CNF_Y Δ39-426) are still able to promote cell binding and endosomal uptake as indicated by colocalization studies (Figs 2D and 4).

In *E. coli* CNF1, the binding site for the Lu/BCAM receptor was shown to include amino acids 720-730 of the catalytic domain (Reppin *et al*, 2017). The respective segment is significantly different in CNF_Y (Fig EV1), which may explain why CNF_Y does not interact with Lu/BCAM. Instead, a recent study has shown that a C-terminal fragment of CNF_Y (residues 709-1014) employs glycosaminoglycans as receptors and is sufficient for endosomal uptake (Kowarschik *et al*, 2020), in line with the observations made here. Thus CNF_Y, similar to CNF1 (Piteau *et al*, 2014; Reppin *et al*, 2017), contains two distinct host cell binding sites, one each at the N- and C-terminus. In CNF_Y, these binding sites enable endosomal uptake independently of each other, and the presence of two receptor binding sites might broaden the range of targeted cells or may increase host cell binding affinity.

The D4-5 segment adopts a different conformation and shows increased deamidase activity after cleavage from full-length CNF_Y

Previous work with *E. coli* CNF1 demonstrated that translocation releases a fragment consisting of the ART-like domain D4 and the deamidase domain D5 into the cytosol of host cells (Knust *et al*, 2009). This prompted us to crystallize the respective segment of CNF_Y, leading to a structure in which linker residues V702-L717 again were too flexible to be traced and in which the two domains adopt a different relative orientation with respect to the full-length protein. Whereas D4 and D5 interacted only weakly in the complete toxin, they now engage in a large interface (1100 $Å^2$), whereby the active site crevice of D5 is extended by D4 and becomes fully solvent-exposed (Fig 7A). To reach this position, domain D4 has to rotate by more than 140°, which can probably only be achieved after cleavage from D1-3

and through the flexibility of the linker connecting both domains. The contact area between both domains in the free D4-5 subunit overlaps largely with that of D3-5 in the full-length structures such that both conformations are mutually exclusive, i.e. the D4-5 subunit cannot adopt the conformation observed in the free state when it is bound to D1-3.

The finding that the active site within domain D5 becomes more exposed in the recombinant D4-5 fragment suggested that presence of domains D1-3 may repress the deamidase activity of CNF_Y and that cleavage of the D4-5 fragment is required to rearrange and liberate and activate the catalytic unit. To test this hypothesis, we incubated equal amounts of purified CNF_Y 1-1014 (D1-5) and CNF_Y 526-1014 (D4-5) with host cell extracts or recombinant RhoA and analyzed the deamidation of RhoA in gel-shift assays and with proteomic methods. As shown in Fig 7B-C, RhoA deamidation by CNF_Y 526-1014 (D4-5) protein was indeed significantly faster than by the full-length protein, indicating that the domain rearrangement seen in the D4-5 fragment enhances the deamidase activity and that the full-length toxin is in an autoinhibited state with respect to this activity.

Discussion

Here we show that CNF_Y and related CNFs consist of five individual structural building blocks that enable the different steps of the intoxication process, namely secretion, cell attachment, entry, translocation and enzymatic activity. The three N-terminal domains D1-3 all possess novel folds and constitute the secretion and membrane translocation unit, whereas the two C-terminal domains D4-5 form the toxicity-mediating unit of the toxin. We further show that the D1-3 unit is sufficient to transport cargo proteins such as β-lactamase into the cytosol of host cells. Strikingly, both the Rho deamidation and β-lactamase activity were preserved when the reporter was fused to the C-terminal end of the full-length protein (Fig 3), indicating that the secretion and transport module of the CNF_Y protein is very robust and insensitive to C-terminal extensions, making it an attractive tool for drug delivery.

The molecular mechanisms by which domains D1-3 promote the delivery of the cargo from the bacterial to the host cell cytosol are still unknown. However, considering the

compact arrangements of the modules with large hydrophobic interfaces between domains D1 and D2, D3 and D4, as well as D3 and D5, it is likely that the full-length toxin is secreted from the bacterial cell and endocytosed by the host cells as monolithic compact structure. In fact, the CNF_Y toxin has recently been identified on the surface of outer membrane vesicles (OMVs) isolated from *Y. pseudotuberculosis* culture supernatants (Monappa et al. 2018). While this could indicate that the toxin might be predominantly delivered into endosomes by OMVs, our data further show that also the purified CNF_Y toxin interacts with and is efficiently internalized into host cells on its own. This suggests that the toxin is also directly secreted by the bacterial cell and/or exposed on the OMVs to promote contact with target cells.

The data presented here further show that the cellular toxin uptake process not only requires segments identified for receptor binding in D2 and for translocation in D1, but also the imperfect β-barrel domain D3. It is interesting to note that D1 is, due to its mostly α-helical character, reminiscent of the translocation machinery of other toxins including that of the diphtheria toxin DT. DT, CNFs and several other AB-type toxins contain two hydrophobic stretches that are believed to fold into α-helices and insert into the endosomal membrane after charge neutralization of surrounding acidic residues (Pei *et al*, 2001; Orrell *et al*, 2017). In CNF_Y, the respective residues 350 – 372 and 387 – 412 were not found in the predicted α-helical structure (Fig 1B). However, since the crystal structures presented here have been obtained at neutral pH, it is conceivable that this region undergoes refolding during endosomal acidification. While the precise molecular mechanism of the complex translocation process of CNF_Y is still unclear (Pitard & Malliavin, 2019), work with DT suggests that the catalytic subunit of this toxin is unfolded in the translocation process (Murphy, 2011). The fact that (i) translocation in CNFs also involves two hydrophobic motifs interrupted by acidic residues and (ii) the observation that a sequence that gets cleaved to release the catalytic unit (D4-5) of CNF (residues 532 to 544) is not accessible in the full-length structure (Fig 1C) may hint at a similar unfolding in the CNFs. In this respect, the similarity of parts of the CNF_Y's D1 domain to the putative translocation domain of nigritroxin

(Fig 5A) (Labreuche *et al*, 2017) is interesting, because the translocation domain of this toxin does not contain hydrophobic α-helices. This could indicate that the translocation process occurs through several steps that involve different parts of the translocation machinery, most of which are not shared between the CNFs and nigritoxin.

Sequence searches in the UniRef50 database (Suzek *et al*, 2015) revealed that large sections of the D1-3 domain of CNF_Y are also found in a number of un- or less characterized bacterial proteins, suggesting that these proteins are toxins that apparently utilize a similar secretion and translocation device for their catalytic domains (Fig 8). For example, about 530 amino acids of the N-terminus of CNF_Y share between 30-50% sequence identity to the N-terminus of *Pasteurella multocida* toxin PMT (Bergmann *et al*, 2013). Moreover, members of a group consisting of 372 proteins with approximately 900 residues each were found to possess a canonical RSE-type ART-domain at their C-terminus (represented by UniProt entry A0A0P9UH04 from *Pseudomonas syringae pv. maculicola*) in addition to a CNF-like translocation apparatus. A second group of 206 proteins with more than 1000 residues contains a C-terminal glycosyltransferase (represented by UniProt entry A0A0N8SZE6 from *Pseudomonas syringae pv. syringae*). Since the C-termini of these proteins differ from CNF_Y (Fig 8), it is likely that the toxins consist of individual modules that have been shuffled in the course of evolution. This aligns with a recent analysis of the distribution of CNF-like deamidase domains, which are also found at different positions within the sequence of other toxins or as stand-alone proteins (Cruz-Migoni *et al*, 2011; Ho *et al*, 2018).

The finding that the DUF4765 domain D4 shows similarity to ADP-ribosyltransferases was surprising and led us to investigate if the released D4-5 may possess an additional and previously unrecognized enzyme activity that may contribute to the toxicity of CNFs. However, the observation that CNF_Y toxicity strictly depended on the activity of the deamidase D5 domain whereas mutations of the potential/suggested NAD^+ binding domain within D4 had no effect (Appendix Fig S5), together with the fact that we could not detect NAD^+ binding in biophysical experiments, speaks against such an additional activity. On the other

hand, the NAD^+ affinity of some ADP-ribosyl transferases is very low. This is exemplified by cholera toxin, where a K_D of 4.0 ± 0.4 mM has been determined (Galloway & van Heyningen, 1987). Alternatively, the grossly different and mutually exclusive relative orientations of the D4 and D5 domains in the free D4-5 subunit with respect to the full-length CNF_Y structure (Fig 7) could suggest that D4 may have a regulatory role. On the one hand, the finding that the active site becomes solvent-accessible and that the crevice leading to the active site of D5 becomes extended by parts of D4 (Fig 7) could fine-tune the deamidase function of D5 with respect to general activity levels or substrate specificity towards RhoA, Rac1 or Cdc42. On the other hand, D4 could contribute to localizing the catalytical unit within the host cell by promoting access to membrane-associated Rho GTPases. In fact, CNFs act predominantly on Rho GTPases bound to GTP, a form essentially found at the cytoplasmic face of the host cell membrane (Boquet, 2001). Clearly, the importance of D4 merits future studies.

In summary, the data presented here provide insight into the full-length and released active D4-5 structure, and they illustrate the importance of the individual building blocks of CNFs and related exotoxins. This not only forms the basis for the detailed analysis of the molecular secretion and transport mechanism, but also enables the rational design of the transport module as a toxin-based cargo delivery tool for cytosolic drug/therapeutics delivery and the structure-guided development of inhibitors of CNF-like virulence factors.

Materials and Methods

Bacterial strains, cell lines, plasmids and growth conditions

All bacterial strains and plasmids used in this study are listed in Appendix Tab S3. All oligonucleotide primers used for cloning are listed in Appendix Tab S4. *E. coli* strains were grown in Luria-Bertani (LB; Becton Dickinson) broth at 37°C. *Yersinia* strains were aerobically grown in LB at 25°C or 37°C. Other media used for bacterial growth were brain-heart infusion broth (BHI) (Gibco) and Double Yeast Tryptone medium (DYT) (Gibco). Cultures were supplemented with 30 µg/ml kanamycin (Kan) or chloramphenicol (Cm) where necessary. HEp-2 cells (ATCC CCL-23) were grown at 37°C, 5% CO_2 in RPMI (Gibco) supplemented with 7.5% newborn calf serum (NCS; Sigma).

Antibodies

The following antibodies have been used in this study: anti RhoA from Biomol No. NB-26007 and Abcam No. ab54835; anti-actin from Sigma No. A2228-100UL, anti-3x-Flag from Sigma No. F3165-1MG, anti-beta lactamase (TEM) from Abcam No. ab12251, anti-GFP from Sigma No. 11814460001, and anti-IgG from Cell Signalling No. 7076S.

Cloning, expression and purification of recombinant CNF_Y variants

For crystallography purposes, truncated constructs were generated comprising a fragment lacking the catalytically active C-terminal domain (CNF_Y1-704), a construct containing both C-terminal domains D4-5 (CNF_Y526-1014) and another containing only the catalytic domain D5 (CNF_Y720-1014). For crystallization of the full-length protein, a construct containing the inactive C866S variant of CNF_Y was produced.

The coding sequences of D4-5 (CNF_Y1-704) and D5 (CNF_Y720-1014) were both cloned into pET28c containing sequences coding for an N-terminal hexa-histidine tag and a thrombin protease cleavage site. The constructs were transformed into *E. coli* BL21 (DE3) (CNF_Y1-704) or Rosetta II (DE3) (CNF_Y720-1014). Native protein was expressed in lysogenic broth (LB) medium at 20°C after induction with 0.5 mM isopropyl-β-D-

thiogalactopyranosid (IPTG) for 16-18 h (D1-4; CNF_Y1-704) or 4 h (D5; CNF_Y720-1024) (5), respectively. Seleno-L-methionine (Se-Met) labeled protein of CNF_Y1-704 (D1-4) was expressed using M9 minimal medium.

After harvesting, the cell pellets were resuspended in lysis-buffer (for D1-4/CNF_Y1-704: 1 x PBS, 400 mM NaCl, 5 mM β-mercaptoethanol, 5 mM $MgSO_4$, 10 mM imidazole; for D5/CNF_Y720-1014: 50 mM Tris/HCl pH 8.0, 400 mM NaCl, 5 mM imidazole) and lysed by sonification. The supernatant after centrifugation was mixed with 1 ml Ni-NTA resin pre-equilibrated with wash I buffer (D1-4/CNF_Y1-704: 1 x PBS, 400 mM NaCl, 10 mM imidazole, 5 mM MgSO4, 5 mM β-mercaptoethanol; D5/CNF_Y720-1014: 50 mM Tris/HCl pH 8, 400 mM NaCl, 5 mM imidazole) and incubated for 1 h on an overhead-shaker at 4°C. After washing with wash I buffer and wash II buffer (D1-4/CNF_Y1-704: 1 x PBS, 400 mM NaCl, 20 mM imidazole, 5 mM $MgSO_4$, 5 mM β-mercaptoethanol; D5/CNF_Y720-1014: 50 mM Tris/HCl pH 8, 400 mM NaCl, 20 mM imidazole), elution of the protein was carried out with 12 x 1 ml of elution buffer (D1-4/CNF_Y1-704: 1 x PBS, 400 mM NaCl, 250 mM imidazole, 5 mM MgSO4, 5 mM β-mercaptoethanol; D5/CNF_Y720-1014: 50 mM Tris/HCl, 250 mM NaCl, 250 mM imidazole). Buffer exchange and tag cleavage with thrombin (1:50 mg/mg) were achieved over night by dialysis at 4°C in wash I buffer. To remove cleaved His-Tag, uncleaved protein and the thrombin protease, 1 ml of Ni-NTA resin and 5 ml of benzamidine-sepharose resin, respectively were mixed with the dialyzed protein solution. The collected flow-through predominantly contained pure protein. Further purification was achieved by size-exclusion chromatography. D1-4 (CNF_Y1-704) was purified using a HiLoad 16/600 Superdex 200 pg (GE Healthcare) pre-equilibrated in buffer containing 20 mM Tris pH 8.0, 150 mM NaCl, 5 mM DTT. D5 (CNF_Y720-1014) was purified using a HiLoad 16/600 Superdex 75 pg (GE Healthcare) pre-equilibrated in buffer containing 25 mM Tris pH 8.0, 100 mM NaCl. The proteins were then concentrated to 20 mg/ml, flash-frozen in liquid nitrogen and stored or directly used for crystallographic screens.

The gene encoding for the full-length protein of the CNF_Y C866S variant was cloned into a modified pCOLA Duet-1 vector (Novagen) encoding for an N-terminal Strep-tag II and

TEV-protease recognition site (construct: CNF_Y C866S). In the case of D4-5 (CNF_Y 526-1014), the insert was amplified from pCNF$_Y$3xFlag as template so that the three C-terminal FLAG-epitopes were included in the insert and cloned into the same modified pCOLA Duet-1 vector that was also used for the full-length toxin (construct: pVP-CNF$_Y$526-1014-3xFlag). Both proteins were heterologously expressed in *E. coli* BL21 (DE3) in ZYM-5052 auto-inducing medium (Studier, 2005) at 20°C for 20-24 h.

In the case of D4-5 (CNF$_Y$526-1014), the cell pellet was resuspended in a buffer containing 20 mM HEPES/NaOH pH 7.5, 300 mM NaCl, 2 mM TCEP, one tablet of complete EDTA-free protease inhibitor cocktail (Roche) and lysed by sonication. The protein was isolated from the supernatant after centrifugation for 1 h at 100.000 x g using a self-packed 10 ml column with Strep-Tactin Superflow High Capacity resin (IBA) and eluted from the column with a single step of 5 mM d-desthiobiotin. The affinity tag was cleaved off with TEV protease (1:50 mg/mg) at 4°C overnight. Gel filtration was carried out using a HiLoad 16/600 Superdex 200 pg column (GE Healthcare) in 20 mM HEPES/NaOH pH 7.5, 300 mM NaCl, 2 mM TCEP. The peak fractions were concentrated to 5 mg/ml and flash-frozen in liquid nitrogen for crystallization screening.

For the full-length protein, the cell pellet was resuspended in a buffer containing 20 mM HEPES/NaOH pH 7.5, 100 mM NaCl, 1 mM TCEP, one tablet of complete EDTA-free protease inhibitor cocktail (Roche) and lysed by sonication. The protein was isolated from the supernatant after centrifugation for 1 h at 100.000 x g using a self-packed 10 ml column with Strep-Tactin Superflow High Capacity resin (IBA) and eluted from the column with a single step of 5 mM d-desthiobiotin. The affinity tag was cleaved off with TEV protease (1:50 mg/mg) at 4°C overnight. Gel filtration was carried out using a HiLoad 16/600 Superdex 200 pg column (GE Healthcare) in 20 mM HEPES/NaOH pH 7.5, 100 mM NaCl, 1 mM TCEP. The fractions corresponding to the second peak in the chromatogram (elution volume 70-75 ml) were pooled and subjected to further size exclusion chromatography on a Superdex 200 Increase 10/300 GL column (GE Healthcare) in the same buffer. The peak fractions were concentrated to 27.5 mg/ml and flash-frozen in liquid nitrogen for crystallization

screening. All chromatographic steps were carried out using an Äkta Purifier system (GE Healthcare). The samples were analyzed by SDS-PAGE (12%), and protein concentrations were determined from the absorbances at 280 nM with the extinction coefficients as calculated by Protparam (Gasteiger *et al*, 2003).

CNF_Y-TEM fusion proteins were obtained in a similar manner after cloning into pET28a, overexpression in *E. coli* Rosetta II (DE3) and a two-step purification protocol involving Ni-NTA affinity and size exclusion chromatography.

Crystallization

Crystallization trials were set up at room temperature with a HoneyBee 961 crystallization robot (Digilab Genomic Solutions) in Intelli 96-3 plates (Art Robbins Instruments) with 200 nl protein solution at different concentrations and 200 nl reservoir solution. Native D1-4 (CNF_Y1-704) was crystallized in 0.1 M Tris pH 7.3-7.9, 0.2 M ammonium sulfate and 19-21% (w/v) PEG 5000 MME. The Se-Met derivative of D1-4 (CNF_Y1-704) was crystallized in 0.1 M tri-sodium citrate pH 5.9-6.2, 0.2 M ammonium acetate and 28-32% (w/v) PEG 4000. Macro-seeding was applied in order to obtain well-diffracting crystals. As all tested compounds for cryoprotection were not tolerated by the samples, the crystals were flash-cooled without any additional cryoprotection. The catalytic domain D5 (CNF_Y720-1014) yielded crystals in several PEG or ammonium sulfate containing conditions and the best diffracting crystals were obtained in 0.2 M ammonium fluoride with 20% (w/v) PEG 3350. Crystals were cryo-protected with either 25% glycerol or 100% Type A oil (Hampton Research) prior to flash freezing in liquid nitrogen. A single well-diffracting crystal of D4-5 (CNF_Y526-1014) was obtained in the presence of 1 mM ATP in a condition containing 0.24 M magnesium chloride, 22.5% (w/v) PEG 2000 monomethyl ether. The crystal was harvested after 130 days of growth and cryo-protected by addition of 10% (v/v) (2*R*,3*R*)-2,3-butanediol. A single crystal of sufficient diffraction quality of full-length CNF_YC866S was obtained in 1.4 M ammonium sulfate, 0.13 M lithium acetate, 0.1 M HEPES/NaOH pH 7.1.

The crystal was harvested after 21 days of growth and after removal of satellite crystals cryo-protected by addition of 10% (v/v) (2*R*,3*R*)-2,3-butanediol.

Data collection and processing

Data collection of native and Se-Met-derivatized D1-4 (CNF_Y 1-704) was performed on beamline PXIII of the Swiss Light Source (Paul Scherrer Institute, Villigen, Switzerland) and BESSY BL14.1 (Helmholtz Zentrum Berlin, Germany) (Mueller *et al*, 2015). High-resolution data of D5 (CNF_Y 720-1014) were recorded at beamline BL 14.2 of the BESSY II (Helmholtz-Zentrum Berlin, Germany). Datasets of domain D4-5 (CNF_Y 526-1014) and full-length CNF_YC866S were measured at beamline X06DA (PXIII) at the Swiss Light Source (Paul Scherrer Institute, Villigen, Switzerland). Data processing was achieved either manually via the XDS software package (Kabsch, 2010) or by using the AutoPROC (Vonrhein *et al*, 2011) toolbox (Global Phasing) executing XDS (Kabsch, 2010), Pointless (Evans, 2006), and Aimless (Evans & Murshudov, 2013). All datasets were recorded at a temperature of 100 K.

Structure determination, refinement and model building.

The structure of domain D1-3 (CNF_Y 1-704) was solved by single anomalous dispersion (SAD) using data collected at the selenium absorption edge. The initial phases were calculated using AutoSol (Terwilliger *et al*, 2009) and a partial model was generated running AutoBuild (Terwilliger *et al*, 2008), both components of the Phenix software package (Adams *et al*, 2010). The output model was analyzed in Coot (Emsley *et al*, 2010) and misplaced main chains were removed or corrected manually in order to obtain a reliable search-model for the following molecular replacement procedures against the dataset of native D1-4 (CNF_Y 1-704) and the full-length C866S variant. The structure of D5 (CNF_Y 720-1014) was determined by molecular replacement using the structure of the catalytic C-terminal domain of CNF1 from *E. coli* (PDB: 1HQ0, (Buetow *et al*, 2001)) as search-model. The structure of domain D4-5 (CNF_Y526-1014) was determined by molecular replacement

using the structure of domain D5 (CNF_Y 720-1014) and the region comprising residues 526-704 from domain D1-4 (CNF_Y 1-704). Phases for full-length CNF_YC866S were obtained by using both domain D1-4 (CNF_Y1-704) and D5 (CNF_Y720-1014) as search-models in molecular replacement. The molecular replacement procedures were carried out using Phaser (McCoy *et al*, 2007) from the Phenix suite (Adams *et al*, 2010). The structural models were built using Coot (Emsley *et al*, 2010) and crystallographic refinement was performed with Phenix.refine (Afonine *et al*, 2012) including the addition of hydrogens in riding positions and TLS-refinement. 5% of random reflections were flagged for the calculation of R_{free}. The model of domain D1-4 (CNF_Y 1-704) was at 3.3 Å resolution and refined to R/R_{free} of 24/27% in space group $P2_1$. The structure of domain D5 (CNF_Y720-1014) was at 1.1 Å resolution and refined to R/R_{free} of 17/18% in space group $P2_1$. The structure of domain D4-5 (CNF_Y526-1014) was at 1.8 Å resolution and refined to R/R_{free} of 16/19% in space group $P2_12_12_1$. The structural model of the full-length C866S variant of CNF_Y was at 2.7 Å resolution and refined to R/R_{free} of 21/24% in space group $I2_12_12_1$. Data collection and refinement statistics are summarized in Tab EV1. Figures of crystal structures were prepared using the PyMOL Molecular Graphics System version 2.0.0 (Schrödinger, LLC).

Construction of fusion plasmids and C-terminal *cnfY* deletions

To construct the plasmids for CNF_Y fusion proteins, the *blaM* gene and the 3xFlag tag were amplified using primers listed in Appendix Tab S4. pFU189 was used as a backbone from which the *luxCDABE* operon was removed by digestion with *Pst*I and *Not*I after which *blaM* or the 3xFlag tag were ligated into the vector, resulting in pTEM and p3xFLAG, respectively.

The PCR fragments of C-terminal *cnfY* deletions containing the *cnfY* promoter region were cloned into the *Bam*HI and *Pst*I sites of pTEM and p3xFLAG using the Quick-Fusion cloning kit (Biotool) with primers listed in Appendix Tab S4. For the construction of $pCNF_Y$-GFP, *gfp* was excised from pFU31 and ligated into the *Pst*I and *Not*I sites of digested $pCNF_Y$-TEM. All clones were transformed into *E. coli* DH10β and confirmed by sequencing.

Structure-function analysis of CNF_Y

The plasmids were electroporated into *Y. pseudotuberculosis* YP147 (Δ*cnfY*) and selected for on LB agar plates containing the appropriate antibiotics.

Site-directed mutagenesis of *cnfY*

Single residue mutants were generated by site-directed mutagenesis with primers listed in Appendix Tab S4. $pCNF_Y$-TEM, $pCNF_Y$-3xFLAG were used as templates. Clones were selected on LB containing the appropriate antibiotics. Mutations were verified by DNA sequencing.

Detection of fusion proteins by immunoblotting

For protein expression, strain YP147 harboring the overexpression plasmids encoding full-length CNF_Y or the deletion variants was grown in BHI at 25°C overnight. Cells were harvested by centrifugation at 6,500 rpm and 4°C for 5 min. Cell pellets were washed with PBS and resuspended with lysis buffer (50 mM Tris-HCl pH 7.5, 100 mM NaCl, 5 mM $MgCl_2$, 0.3% Triton X-100, 3 mg/ml lysozyme and protease inhibitor cocktail). After incubation at room temperature for 1 h, protein samples were centrifuged for 10 min and supernatants were sterilized with a 0.2 µm filter. To detect proteins, Western blot analysis was performed. The proteins were separated on a 10% SDS-polyacrylamide gel and transferred onto an Immobilon PVDF membrane (Millipore). Membranes were blocked in 5% BSA/TBST at 4°C overnight. Subsequently, the membrane was washed and incubated with primary antibody diluted in 5% BSA/TBST (1:10,000 anti-Flag (Sigma-Aldrich) or anti-Beta lactamase (Abcam)) at room temperature for 1 h. After washing, the secondary antibody diluted in 5% skim milk/TBST (1:5,000 anti-mouse IgG HRP (Cell Signaling Technology)) was added for 30 min at room temperature. After washing the membrane, proteins were visualized using the Western Lightning ECL II Kit (Perkin Elmer) and exposed on X-Ray film (GE Healthcare Amersham Hyperfilm ECL, Fisher Scientific).

Nitrocefin secretion assay

Bacteria were grown overnight at 25°C in BHI containing the appropriate antibiotics. Subsequently, equal amounts of bacteria were pelleted by centrifugation at 13,000 rpm for 10 min. 95 µl of each supernatant was transferred to a 96-well plate in triplicate. 5 µl nitrocefin (2 mM) were added to each well and the plate was incubated at room temperature for 30 min. Beta-lactamase activity was determined at 390 nm (yellow) and 486 nm (red) using a VarioSkan plate reader (Thermo Scientific).

Microbial viability assay

The microbial viability was assessed in equalized bacterial cultures using the BacTiter-Glo™ Microbial Cell Viability Assay kit (Promega) according to the manufacturer's recommendations and luminescence was measured using a VarioSkan plate reader (Thermo Scientific).

Fluorescent actin staining

HEp-2 cells were seeded onto coverslips at a concentration of $5x10^4$ cells/well and allowed to attach overnight. The next day, cells were washed and incubated with an equal amount of cleared bacterial cell lysates for 24 h at 37°C, 5% CO_2. After washing with PBS, cells were fixed in 4% paraformaldehyde for 15 min at room temperature. Subsequently, washed cells were permeabilized with 0.1% Triton X-100 in PBS for 1 min. The actin cytoskeleton was stained with FITC- or TRITC-Phalloidin (0.5 µg/ml in PBS; Sigma-Aldrich) and mounted on slides using ProLong® Gold Antifade mounting medium containing DAPI (Thermo scientific). Cells were visualized by fluorescence microscopy using an Axiovert II inverted fluorescence microscope (Carl Zeiss) with Axiocam HR and the AxioVision program (Carl Zeiss).

CNF_Y translocation assay

In order to study the CNF_Y translocation into the host cells, a β-lactamase (TEM) reporter assay was performed using the LiveBLAzer-FRET B/G Loading Kit (Life Technologies). HEp-2 cells were seeded in 8-well µ-slides (Ibidi) at a concentration of $1.7x10^4$ cells/well and allowed to attach overnight. The next day, cells were washed and incubated for 24 h at 37°C, 5% CO_2 with 20 µg/ml cleared lysates of *Y. pseudotuberculosis* expressing the different CNF_Y-TEM fusion proteins. Cells were washed with PBS, followed by the addition of fresh media containing 20 mM HEPES. Cells were then stained with loading dye according to the manufacturer´s protocol. After staining for 1 h at room temperature, translocation was visualized by fluorescence microscopy using an Axiovert II with Axiocam HR and the AxioVision program (Carl Zeiss).

For the analysis of the translocation dynamics of CNF_Y 1-1014 and CNF_Y 1-526, surface-attached HEp-2 cells were charged with CCF4-AM in the dark for 1 h at 37°C and the change of fluorescence was immediately followed after addition of the respective CNF_Y-TEM fusion construct in *Y. pseudotuberculosis* lysates (20 µg/ml) or the purified recombinant proteins (200 nM), using a CLARIOstar Plus fluorometer (BMG Labtech) or a Cytation 5 plate reader (Biotek), respectively.

Fluorescence microscopy to visualize endocytosis

To test whether the CNF_Y deletion constructs are able to enter the cells through the endocytotic pathway, CellLight® Early or late Endosomes-RFP, BacMam 2.0 (Thermo Scientific) were used to investigate toxin entry to the host cells. HEp-2 cells were seeded $5x10^4$ cells/ml onto coverslips in 24 well plates and allowed to attach overnight. The next day, CellLight® reagent was added to HEp-2 cells around 20 particles per cells for 16 h and the cells were then incubated with CNF_Y toxin on ice for 30 min. Subsequently, cells were washed and transferred to 37°C for 30, 90 or 180 min. To investigate colocalization of CNF_Y with early or late endosome, cells were then fixed and visualized by using a fluorescence

microscope (Axiovert II with Axiocam HR, Carl Zeiss) and the AxioVision program (Carl Zeiss).

Biochemical analysis of RhoA deamidation

Cells were seeded in 10 cm cell culture dishes at the concentration of 2.2 x 10^6 cells/dish and allowed to attach overnight. The next day, cells were washed and incubated for 4 h with 20 µg/ml of cleared lysates from *Y. pseudotuberculosis* expressing different CNF_Y derivatives at 37°C, 5% CO_2. Cells were washed with cold PBS and lysed in 150 µl lysis buffer containing 50 mM Tris-HCl (pH7.4), 100 mM NaCl, 2 mM $MgCl_2$, 10% NP-40 and 0.5 mM phenyl-methyl-sulfonyl fluoride (PMSF). Cells were then scraped off and centrifuged for 30 min (13,000 rpm, 4°C). Sodium dodecyl sulfate (SDS) sample buffer was added to the clear lysates and samples were separated on 12% SDS-gel. After blotting onto a PVDF membrane, RhoA was detected using mouse anti-RhoA IgG (Millipore) (1:1000) as a primary antibody and followed by secondary antibody goat anti-mouse IgG-HRP (Cell signaling). Membranes were visualized using the Western Lightning ECL II Kit (Perkin Elmer) and exposed on X-Ray film.

***In vitro* RhoA shift assay**

In vitro RhoA shift assays were performed in order to check for proper folding and catalytic activity of CNF_Y deletion constructs. Cells were seeded on 150 mm dish at the concentration of 5 x 10^6 cells/dish and allowed to attach overnight. The next day, cells were washed with PBS and lysed in 300 µl lysis buffer (50 mM Tris-HCl, pH 7.5, 5 mM $MgCl_2$, 1 mM EDTA, 10% NP-40 and 1 mM dithiothreitol (DTT)). Cells were then scraped off and centrifuged 13,000 rpm at 4°C for 30 min. 20 µg/ml of cleared lysates from *Y. pseudotuberculosis* expressing different CNF_Y derivatives were added to the prepared cell extracts and then incubated for 4 h, or 1 µM purified CNF_Y or CNF_Y 526-1014 protein were incubated in the cell extracts for 10-60 min at 37°. The reactions were stopped by adding SDS-sample buffer

and heated at 95°C for 10 min. Samples were then subjected to 12% SDS-PAGE. After blotting onto a PVDF membrane, blots were developed as mentioned above.

Quantification of RhoA deamidation by mass spectrometry

Recombinant RhoA (20 µM) was incubated at 37°C with full-length CNF_Y or CNF_Y 526-1014 in 100 µl assay-buffer (20 mM HEPES/NaOH, 300 mM NaCl, 2 mM $MgCl_2$, 2 mM TCEP, 100 µM GDP). Samples, after setup for 30 min, 3 h and 16 h, were immediately mixed with 2-fold SDS-PAGE loading buffer, denatured for 5 min at 95°C and subjected to SDS-PAGE by applying 2 µg of RhoA per lane. After staining with Coomassie Blue, bands corresponding to RhoA were cut out, destained with 30% acetonitrile in 50 mM TEAB and then dehydrated with 100% acetonitrile. After reduction with 20 mM TCEP in 50 mM TEAB (1 h, 56°C), alkylation was performed by 20 mM MMTS in 50 mM TEAB (1 h, RT), followed by in-gel digestion over night with 50 ng trypsin (Promega) in 50 mM TEAB. Peptides were extracted by using 10 gel volumes of 0.5% formic acid in 30% acetonitrile, vacuum dried and resuspended in 0.1% formic acid before applying to Evotips as recommended by the manufacturer (Evosep). Peptide sequencing of RhoA was carried out by tandem mass spectrometry on an Evosep One HPLC system linked with a timsTOF Pro mass spectrometer (Bruker). Separation of modified peptide ions was supported by ion mobility and RhoA deamidation in the peptide QVELALWDTAGQEDYDR was identified by using PEAKS 10+ software. Deamidated and corresponding non-deamidated RhoA peptide variants were manually validated at the level of their distinct HPLC-retention times and corresponding representative fragmentation spectra (MS2; Data Analysis, Bruker). RhoA modification was then quantified by selected ion chromatograms (MS1; Data Analysis, Bruker). CNF_Y-dependent deamidation was determined in comparison to non-treated RhoA samples (negative control) and based on the area under peaks for double charged non-deamidated peptides (m/z 1004.9645 ± 0.005) and deamidated peptides (retention time + 0.3 min, m/z 1005.4590 ± 0.005).

References

Adams PD, Afonine PV, Bunkóczi G, Chen VB, Davis IW, Echols N, Headd JJ, Hung L-W, Kapral GJ, Grosse-Kunstleve RW, McCoy AJ, Moriarty NW, Oeffner R, Read RJ, Richardson DC, Richardson JS, Terwilliger TC & Zwart PH (2010) PHENIX: a comprehensive Python-based system for macromolecular structure solution. *Acta Crystallogr. D Biol. Crystallogr* **66:** 213–221

Afonine PV, Grosse-Kunstleve RW, Echols N, Headd JJ, Moriarty NW, Mustyakimov M, Terwilliger TC, Urzhumtsev A, Zwart PH & Adams PD (2012) Towards automated crystallographic structure refinement with phenix.refine. *Acta Crystallographica Section D Biological Crystallography* **68:** 352–367

Aleksiev T, Potestio R, Pontiggia F, Cozzini S & Micheletti C (2009) PiSQRD: a web server for decomposing proteins into quasi-rigid dynamical domains. *Bioinformatics* **25:** 2743–2744

Bergmann S, Jehle D, Schwan C, Orth JHC & Aktories K (2013) Pasteurella multocida Toxin as a Transporter of Non-Cell-Permeating Proteins. *Infection and Immunity* **81:** 2459–2467

Berman HM, Westbrook J, Feng Z, Gilliland G, Bhat TN, Weissig H, Shindyalov IN & Bourne PE (2000) The Protein Data Bank. *Nucleic Acids Res* **28:** 235–242

Blumenthal B, Hoffmann C, Aktories K, Backert S & Schmidt G (2007) The cytotoxic necrotizing factors from Yersinia pseudotuberculosis and from Escherichia coli bind to different cellular receptors but take the same route to the cytosol. *Infect. Immun.* **75:** 3344–3353

Boquet P (2001) The cytotoxic necrotizing factor 1 (CNF1) from Escherichia coli. *Toxicon* **39:** 1673–1680

Buetow L, Flatau G, Chiu K, Boquet P & Ghosh P (2001) Structure of the Rho-activating domain of Escherichia coli cytotoxic necrotizing factor 1. *Nat. Struct. Biol.* **8:** 584–588

Buetow L, Flatau G, Chiu K, Boquet P & Ghosh P (2002) Strategies for the structural determination of the catalytic domain of Escherichia coli cytotoxic necrotizing factor 1. *Acta Crystallogr D Biol Crystallogr* **58:** 366–9

Cavaillon J-M (2018) Exotoxins and endotoxins: Inducers of inflammatory cytokines. *Toxicon* **149:** 45–53

Chung JW, Hong SJ, Kim KJ, Goti D, Stins MF, Shin S, Dawson VL, Dawson TM & Kim KS (2003) 37-kDa laminin receptor precursor modulates cytotoxic necrotizing factor 1-mediated RhoA activation and bacterial uptake. *J. Biol. Chem.* **278:** 16857–16862

Clemons NC, Bannai Y, Haywood EE, Xu Y, Buschbach JD, Ho M & Wilson BA (2018) Cytosolic Delivery of Multidomain Cargos by the N Terminus of Pasteurella multocida Toxin. *Infect. Immun.* **86:**

Cohen MS & Chang P (2018) Insights into the biogenesis, function, and regulation of ADP-ribosylation. *Nat. Chem. Biol.* **14:** 236–243

Cruz-Migoni A, Hautbergue GM, Artymiuk PJ, Baker PJ, Bokori-Brown M, Chang C-T, Dickman MJ, Essex-Lopresti A, Harding SV, Mahadi NM, Marshall LE, Mobbs GW, Mohamed R, Nathan S, Ngugi SA, Ong C, Ooi WF, Partridge LJ, Phillips HL, Raih MF, et al (2011) A Burkholderia pseudomallei toxin inhibits helicase activity of translation factor eIF4A. *Science* **334:** 821–824

Diabate M, Munro P, Garcia E, Jacquel A, Michel G, Obba S, Goncalves D, Luci C, Marchetti S, Demon D, Degos C, Bechah Y, Mege JL, Lamkanfi M, Auberger P, Gorvel JP, Stuart LM, Landraud L, Lemichez E & Boyer L (2015) *Escherichia coli* alpha-

hemolysin counteracts the anti-virulence innate immune response triggered by the Rho GTPase activating toxin CNF1 during bacteremia. *PLoS Pathog* **11:** e1004732

Diana G, Valentini G, Travaglione S, Falzano L, Pieri M, Zona C, Meschini S, Fabbri A & Fiorentini C (2007) Enhancement of learning and memory after activation of cerebral Rho GTPases. *Proc. Natl. Acad. Sci. U.S.A.* **104:** 636–641

Emsley P, Lohkamp B, Scott WG & Cowtan K (2010) Features and development of Coot. *Acta Crystallogr. D Biol. Crystallogr.* **66:** 486–501

Evans P (2006) Scaling and assessment of data quality. *Acta Crystallogr. D Biol. Crystallogr.* **62:** 72–82

Evans PR & Murshudov GN (2013) How good are my data and what is the resolution? *Acta Crystallogr. D Biol. Crystallogr.* **69:** 1204–1214

Fabbri A, Gauthier M & Boquet P (1999) The 5' region of cnf1 harbours a translational regulatory mechanism for CNF1 synthesis and encodes the cell-binding domain of the toxin. *Mol. Microbiol.* **33:** 108–118

Fabbri A, Travaglione S, Ballan G, Loizzo S & Fiorentini C (2013) The cytotoxic necrotizing factor 1 from E. coli: a janus toxin playing with cancer regulators. *Toxins (Basel)* **5:** 1462–1474

Fabbri A, Travaglione S, Maroccia Z, Guidotti M, Pierri CL, Primiano G, Servidei S, Loizzo S & Fiorentini C (2018) The Bacterial Protein CNF1 as a Potential Therapeutic Strategy against Mitochondrial Diseases: A Pilot Study. *Int J Mol Sci* **19:**

Fabbri A, Travaglione S, Rosadi F, Ballan G, Maroccia Z, Giambenedetti M, Guidotti M, Ødum N, Krejsgaard T & Fiorentini C (2019) The Escherichia coli protein toxin cytotoxic necrotizing factor 1 induces epithelial mesenchymal transition. *Cell. Microbiol.***:** e13138

Falzano L, Fiorentini C, Donelli G, Michel E, Kocks C, Cossart P, Cabanie L, Oswald E & Boquet P (1993) Induction of phagocytic behaviour in human epithelial cells by *Escherichia coli* cytotoxic necrotizing factor type 1. *Mol Microbiol* **9:** 1247–54

Fieldhouse RJ & Merrill AR (2008) Needle in the haystack: structure-based toxin discovery. *Trends Biochem. Sci.* **33:** 546–556

Flatau G, Lemichez E, Gauthier M, Chardin P, Paris S, Fiorentini C & Boquet P (1997) Toxin-induced activation of the G protein p21 Rho by deamidation of glutamine. *Nature* **387:** 729–733

Fournout S, Dozois C, Odin M, Desautels C, Pérès S, Hérault F, Daigle F, Segafredo C, Laffitte J, Oswald E, Fairbrother J & Oswald I (2000) Lack of a role of cytotoxic necrotizing factor 1 toxin from Escherichia coli in bacterial pathogenicity and host cytokine response in infected germfree piglets. *Infect Immun.* **68:** 839–847

Galloway TS & van Heyningen S (1987) Binding of NAD+ by cholera toxin. *Biochem. J.* **244:** 225–230

Gasteiger E, Gattiker A, Hoogland C, Ivanyi I, Appel RD & Bairoch A (2003) ExPASy: The proteomics server for in-depth protein knowledge and analysis. *Nucleic Acids Res.* **31:** 3784–3788

Haywood EE, Ho M & Wilson BA (2018) Modular domain swapping among the bacterial cytotoxic necrotizing factor (CNF) family for efficient cargo delivery into mammalian cells. *J. Biol. Chem.* **293:** 3860–3870

Heine W, Beckstette M, Heroven AK, Thiemann S, Heise U, Nuss AM, Pisano F, Strowig T & Dersch P (2018) Loss of CNFY toxin-induced inflammation drives Yersinia pseudotuberculosis into persistency. *PLoS Pathog.* **14:** e1006858

Ho M, Mettouchi A, Wilson BA & Lemichez E (2018) CNF1-like deamidase domains: common Lego bricks among cancer-promoting immunomodulatory bacterial virulence factors. *Pathog Dis* **76:**

Hodge R & Ridley A (2016) Regulating Rho GTPases and their regulators. *Nat Rev Mol Cell Biol.* **17:** 496–510

Hoffmann C, Aktories K & Schmidt G (2007) Change in substrate specificity of cytotoxic necrotizing factor unmasks proteasome-independent down-regulation of constitutively active RhoA. *J. Biol. Chem.* **282:** 10826–10832

Hoffmann C, Pop M, Leemhuis J, Schirmer J, Aktories K & Schmidt G (2004) The Yersinia pseudotuberculosis cytotoxic necrotizing factor (CNFY) selectively activates RhoA. *J. Biol. Chem.* **279:** 16026–16032

Holm L & Rosenström P (2010) Dali server: conservation mapping in 3D. *Nucleic Acids Res* **38 Suppl:** W545-549

Jørgensen R, Wang Y, Visschedyk D & Merrill AR (2008) The nature and character of the transition state for the ADP-ribosyltransferase reaction. *EMBO Rep.* **9:** 802–809

Kabsch W (2010) XDS. *Acta Crystallogr. D Biol. Crystallogr* **66:** 125–132

Khan NA, Wang Y, Kim KJ, Chung JW, Wass CA & Kim KS (2002) Cytotoxic necrotizing factor-1 contributes to *Escherichia coli* K1 invasion of the central nervous system. *J Biol Chem* **277:** 15607–12

Kim KJ, Chung JW & Kim KS (2005) 67-kDa laminin receptor promotes internalization of cytotoxic necrotizing factor 1-expressing Escherichia coli K1 into human brain microvascular endothelial cells. *J. Biol. Chem.* **280:** 1360–1368

Knust Z, Blumenthal B, Aktories K & Schmidt G (2009) Cleavage of Escherichia coli cytotoxic necrotizing factor 1 is required for full biologic activity. *Infect. Immun.* **77:** 1835–1841

Knust Z & Schmidt G (2010) Cytotoxic Necrotizing Factors (CNFs)-A Growing Toxin Family. *Toxins (Basel)* **2:** 116–27

Koornhof HJ, Smego RA & Nicol M (1999a) Yersiniosis. II: The pathogenesis of *Yersinia* infections. *Eur J Clin Microbiol Infect Dis* **18:** 87–112

Koornhof HJ, Smego RA & Nicol M (1999b) Yersiniosis. II: The pathogenesis of Yersinia infections. *Eur. J. Clin. Microbiol. Infect. Dis.* **18:** 87–112

Kowarschik S, Schöllkopf J, Müller T, Tian S, Knerr J, Bakker H, Rein S, Dong M, Weber S, Grosse R & Schmidt G (2020) Glycosaminoglycans are specific endosomal receptors for Yersinia pseudotuberculosis Cytotoxic Necrotizing Factor. *bioRxiv***:** 2020.05.18.101790

Krissinel E & Henrick K (2007) Inference of Macromolecular Assemblies from Crystalline State. *Journal of Molecular Biology* **372:** 774–797

Labreuche Y, Chenivesse S, Jeudy A, Le Panse S, Boulo V, Ansquer D, Pagès S, Givaudan A, Czjzek M & Le Roux F (2017) Nigritoxin is a bacterial toxin for crustaceans and insects. *Nat Commun* **8:** 1248

Maroccia Z, Loizzo S, Travaglione S, Frank C, Fabbri A & Fiorentini C (2018) New therapeutics from Nature: The odd case of the bacterial cytotoxic necrotizing factor 1. *Biomed. Pharmacother.* **101:** 929–937

McCoy AJ, Grosse-Kunstleve RW, Adams PD, Winn MD, Storoni LC & Read RJ (2007) Phaser crystallographic software. *J Appl Crystallogr* **40:** 658–674

McNichol BA, Rasmussen SB, Carvalho HM, Meysick KC & O'Brien AD (2007) Two domains of cytotoxic necrotizing factor type 1 bind the cellular receptor, laminin receptor precursor protein. *Infect. Immun.* **75:** 5095–5104

Morgan RN, Saleh SE, Farrag HA & Aboulwafa MM (2019) Prevalence and pathologic effects of colibactin and cytotoxic necrotizing factor-1 (Cnf 1) in Escherichia coli: experimental and bioinformatics analyses. *Gut Pathog* **11:** 22

Mueller U, Förster R, Hellmig M, Huschmann FU, Kastner A, Malecki P, Pühringer S, Röwer M, Sparta K, Steffien M, Ühlein M, Wilk P & Weiss MS (2015) The macromolecular crystallography beamlines at BESSY II of the Helmholtz-Zentrum Berlin: Current status and perspectives. *Eur. Phys. J. Plus* **130:** 141

Murphy JR (2011) Mechanism of Diphtheria Toxin Catalytic Domain Delivery to the Eukaryotic Cell Cytosol and the Cellular Factors that Directly Participate in the Process. *Toxins* **3:** 294–308

Orrell KE, Zhang Z, Sugiman-Marangos SN & Melnyk RA (2017) Clostridium difficile toxins A and B: Receptors, pores, and translocation into cells. *Crit. Rev. Biochem. Mol. Biol.* **52:** 461–473

Pei S, Doye A & Boquet P (2001) Mutation of specific acidic residues of the CNF1 T domain into lysine alters cell membrane translocation of the toxin. *Mol. Microbiol.* **41:** 1237–1247

Pitard I & Malliavin TE (2019) Structural Biology and Molecular Modeling to Analyze the Entry of Bacterial Toxins and Virulence Factors into Host Cells. *Toxins (Basel)* **11:**

Piteau M, Papatheodorou P, Schwan C, Schlosser A, Aktories K & Schmidt G (2014) Lu/BCAM adhesion glycoprotein is a receptor for Escherichia coli Cytotoxic Necrotizing Factor 1 (CNF1). *PLoS Pathog.* **10:** e1003884

Popoff MR (2005) Bacterial exotoxins. *Contrib Microbiol* **12:** 28–54

Reppin F, Cochet S, El Nemer W, Fritz G & Schmidt G (2017) High Affinity Binding of Escherichia coli Cytotoxic Necrotizing Factor 1 (CNF1) to Lu/BCAM Adhesion Glycoprotein. *Toxins (Basel)* **10:**

Rippere-Lampe KE, Lang M, Ceri H, Olson M, Lockman HA & O'Brien AD (2001) Cytotoxic necrotizing factor type 1-positive *Escherichia coli* causes increased inflammation and tissue damage to the prostate in a rat prostatitis model. *Infect Immun* **69:** 6515–9

Schmidt G, Sehr P, Wilm M, Selzer J, Mann M & Aktories K (1997) Gln 63 of Rho is deamidated by Escherichia coli cytotoxic necrotizing factor-1. *Nature* **387:** 725–729

Schweer J, Kulkarni D, Kochut A, Pezoldt J, Pisano F, Pils MC, Genth H, Huehn J & Dersch P (2013) The cytotoxic necrotizing factor of Yersinia pseudotuberculosis (CNFY) enhances inflammation and Yop delivery during infection by activation of Rho GTPases. *PLoS Pathog.* **9:** e1003746

Smego RA, Frean J, Koornhof & H. J (1999) Yersiniosis I: Microbiological and clinicoepidemiological aspects of plague and non-plague *Yersinia* infections. *Eur. J. Clin. Microbiol. Infect. Dis.* **18:** 1–15

Studier FW (2005) Protein production by auto-induction in high density shaking cultures. *Protein Expr. Purif.* **41:** 207–234

Suzek BE, Wang Y, Huang H, McGarvey PB & Wu CH (2015) UniRef clusters: a comprehensive and scalable alternative for improving sequence similarity searches. *Bioinformatics* **31:** 926–932

Terwilliger TC, Adams PD, Read RJ, McCoy AJ, Moriarty NW, Grosse-Kunstleve RW, Afonine PV, Zwart PH & Hung LW (2009) Decision-making in structure solution using Bayesian estimates of map quality: the PHENIX AutoSol wizard. *Acta Crystallogr. D Biol. Crystallogr.* **65:** 582–601

Terwilliger TC, Grosse-Kunstleve RW, Afonine PV, Moriarty NW, Zwart PH, Hung LW, Read RJ & Adams PD (2008) Iterative model building, structure refinement and density modification with the PHENIX AutoBuild wizard. *Acta Crystallogr. D Biol. Crystallogr.* **64:** 61–69

Tsurumura T, Tsumori Y, Qiu H, Oda M, Sakurai J, Nagahama M & Tsuge H (2013) Arginine ADP-ribosylation mechanism based on structural snapshots of iota-toxin and actin complex. *Proc. Natl. Acad. Sci. U.S.A.* **110:** 4267–4272

Vannini E, Olimpico F, Middei S, Ammassari-Teule M, de Graaf EL, McDonnell L, Schmidt G, Fabbri A, Fiorentini C, Baroncelli L, Costa M & Caleo M (2016) Electrophysiology of glioma: a Rho GTPase-activating protein reduces tumor growth and spares neuron structure and function. *Neuro-oncology* **18:** 1634–1643

Vonrhein C, Flensburg C, Keller P, Sharff A, Smart O, Paciorek W, Womack T & Bricogne G (2011) Data processing and analysis with the autoPROC toolbox. *Acta Crystallogr. D Biol. Crystallogr.* **67:** 293–302

Walker KE & Weiss AA (1994) Characterization of the dermonecrotic toxin in members of the genus Bordetella. *Infect. Immun.* **62:** 3817–3828

Wolters M, Boyle EC, Lardong K, Trülzsch K, Steffen A, Rottner K, Ruckdeschel K & Aepfelbacher M (2013) Cytotoxic necrotizing factor-Y boosts Yersinia effector translocation by activating Rac protein. *J. Biol. Chem.* **288:** 23543–23553

Zhang Z, Aung KM, Uhlin BE & Wai SN (2018) Reversible senescence of human colon cancer cells after blockage of mitosis/cytokinesis caused by the CNF1 cyclomodulin from Escherichia coli. *Sci Rep* **8:** 17780

Acknowledgements

We thank the beamline staff at the Helmholtz Centre Berlin (Germany) and the Paul Scherrer Institute (Villigen, Switzerland) for providing access to beamlines BL14.1 and BL14.2 at the BESSYII electron storage ring and to beamline X06DA at the SLS synchrotron. Experiments at the SLS have received funding from the European Union's Horizon 2020 research and innovation program under grant agreement n.° 730872, project CALIPSOplus. Andrea Berger and Ute Widow are acknowledged for excellent technical assistance. We thank Janina Schweer for the construction of initial plasmids and strains. Manfred Nimtz and Josef Wissing helped with mass spectrometry experiments. PD and PC received funding from the SFB1009 (Project no. 194468054) of the German Research Foundation (DFG). TH and PC were supported by the HZI Graduate School for Infection Research.

Author contributions

PD and WB conceived the project. PL, EMG and TH produced recombinant proteins and performed crystallization and structure determination. CR, PC, SM, and TS conducted work with *Y. pseudotuberculosis* and analyzed microscopy experiments with eukaryotic cells. Similar microscopy experiments with recombinant proteins were performed by AS, MK and SSD. WJB and LJ performed and analyzed mass-spectrometric experiments. PD, PL, and WB wrote the manuscript.

Data availability

Coordinates and structure factor amplitudes have been deposited in the Protein Data Bank with accession codes 6Q7Z (CNF_Y 1-704), 6Q7Y (CNF_Y 720-1014), 6Q80 (CNF_Y 526-1014) and 6Q7X (CNF_Y 1-1014 C866S).

Competing interests

The authors declare no competing interests.

Figure legends

Figure 1. The crystal structure of CNF_Y from *Y. pseudotuberculosis*.

A Domain boundaries and sequence motifs mapped to the sequence of CNF_Y.

B Cartoon representation of CNF_Y, colored according to domain boundaries determined with PiSQRD (Aleksiev *et al*, 2009). Dark blue: domain D1, cyan: domain D2, dark green: domain D3, yellow: ADP-ribosyltransferase-like domain D4, pink: deamidase domain D5. Other colors indicate the position of sequence motifs that have been identified in *E. coli* CNF1, namely light blue: p37LRP/67LR receptor-binding motif, red: hydrophobic stretches predicted to form membrane-inserting α-helices, orange: cleavage site, magenta: main Lu/BCAM receptor-binding motif. The positions of N- and C-terminus are indicated by N and C, respectively.

C Surface representation of CNF_Y as seen from two different orientations with respect to B. Note that the cleavage site between D3 and D4 (orange) as well as the deamidase active site in D5 are partially blocked in the structure of full-length CNF_Y. The C-terminal domain D5 interacts mainly with D3 (610 $Å^2$), which partially hides the catalytic site of D5, but it interacts only weakly with D4 (380 $Å^2$), which itself establishes an extensive interface with D1 (1390 $Å^2$) by mainly hydrophilic interactions (17 hydrogen bonds and 6 salt bridges).

Figure 2. Synthesis, secretion, and host cell binding of N- and C-terminal deletion variants of CNF_Y.

A Schematic overview of marker-tagged CNF_Y deletion variants.

B 3xFlag-tagged CNF_Y deletion variants were expressed in *Y. pseudotuberculosis* YP147 (Δ*cnfY*) from plasmids under control of their own promoter and were detected in whole cell extracts using an anti-Flag antibody.

C To test secretion of the CNF_Y variants, full-length CNF_Y and different N- and C-terminally deleted variants fused to beta-lactamase (TEM) were expressed in *Y. pseudotuberculosis*

YP147 (Δ*cnfY*). Beta-lactamase activity in the culture supernatant was subsequently measured using nitrocefin as substrate.

D HEp-2 cells remained untreated or were incubated with 20 µg/ml of whole cell extract of *Y. pseudotuberculosis* expressing full-length CNF1, CNF_Y or the N- or C-terminally deleted toxin variants at 37°C for 4 h. The cells were thoroughly washed, pelleted, lysed and the toxin variants bound to the cells were identified by western blotting using an anti-Flag antibody.

Figure 3. Translocation of the deletion variants of CNF_Y and their influence on RhoA activation, actin rearrangements and multinucleation of host cells.

A HEp-2 cells were incubated with 20 µg/ml of whole cell extract of *Y. pseudotuberculosis* expressing full-length CNF_Y or the N- or C-terminally deleted toxin variants fused to β-lactamase (TEM) at 37°C for 4 h. Cleavage of the reporter dye CCF4-AM was used to visualize toxin delivery. After cell entry CCF4-AM is rapidly converted into the negatively charged form CCF4, which is retained in the cytosol and emits a green fluorescence signal (520 nm). In the presence of translocated β-lactamase fusion proteins, CCF4-AM is cleaved, and disruption of FRET results in blue fluorescence (447 nm). White bar: 20 µm.

B Upper panels: HEp-2 cells remained untreated or were incubated with 20 µg/ml of whole cell extract of *Y. pseudotuberculosis* expressing full-length CNF_Y or the N- or C-terminally deleted toxin variants for 4 h. Cells were lysed and the deamidation of RhoA was analyzed by the shift of the modified Rho GTPase band in SDS PAGE gels; lower panel: HEp-2 cells were lysed and the cell extracts were incubated with full-length CNF_Y or the N-terminally deleted toxin variants for 4 h. The deamidation of RhoA in the cell extracts was analyzed by the mobility shift of the modified Rho GTPase on SDS PAGE after detection with anti-RhoA antibodies.

C HEp-2 cells were incubated with 20 µg/ml of whole cell extract of *Y. pseudotuberculosis* expressing full-length CNF_Y or the N- or C-terminally deleted toxin variants for 24 h. The cell nuclei were strained with DAPI (blue) and the actin cytoskeleton was stained using

FITC-phalloidin (green). The formation of large, multinuclear cells was observed by fluorescence microscopy and the formation of thick actin stress fibers and membrane actin folding were only observed with CNF_Y-treated cells. The white scale bar is 40 µm. Cells incubated with extracts of YP147 (Δ*cnfY*) harboring the empty expression vector were used as negative controls.

Figure 4. Localization of the N- and C-terminal deletion variants of CNF_Y in the late endosome.

HEp-2 cells were incubated with 20 µg/ml of whole cell extract of *Y. pseudotuberculosis* expressing full-length CNF_Y, N- or C-terminal deletion variants fused to GFP (green) for 90 or 180 min. Cells were fixed and processed for fluorescence microscopy. The red fluorescent signal represents late endosomes (CellLight Late Endosomes-RFP (Rab7a)). Nuclei were stained with DAPI (blue). A merged image of the different channels is shown, and smaller images are magnified views of boxed areas. White scale bar is 10 µm.

Figure 5. Structural homology of the CNF_Y toxin and domain organization of toxins with a CNF-like translocation apparatus.

A Side-by-side comparison of CNF_Y and nigritoxin. Nigritoxin is a toxin of crustaceans and insects. The translocation domain of nigritoxin (PDB entry 5M41, (Labreuche *et al*, 2017)) and domain D1 of CNF_Y show partial structural similarity (highlighted areas). This similarity was identified with DALI (Holm & Rosenström, 2010) which was also used to align both structures.

B The ART-like domain D4 of CNF_Y. Essential residues of canonical ARTs are not conserved in CNF_Y (RSE-ARTs exemplified by *C. perfringens* iota toxin, PDB entry 4H03 (Tsurumura *et al*, 2013); HYE-ARTs exemplified by *P. aeruginosa* ExoA, PDB entry 2ZIT (Jørgensen *et al*, 2008); carbon atoms of NAD+ shown in black).

C The deamidase domain D5 of CNF_Y. C866 and H881 form a conserved catalytic dyad also found in the deamidase domain of *E. coli* CNF1 (PDB entry 1HQ0, (Buetow *et al*, 2001))

and *Burholderia pseudomallei* lethal factor BLF1 (PDB entry 3TU8, (Cruz-Migoni *et al*, 2011)).

Figure 6. Characterization of mutants in the linker region connecting domain D3 and D4.

A HEp-2 cells were incubated with 20 µg/ml of whole cell extract of *Y. pseudotuberculosis* expressing CNF_Y, the toxin variant mut1: CNF_YI535L/P536A/V537G or mut2: CNF_YI535L/P536A/V537G/F539L/D541A/K542A fused to TEM or no CNF_Y protein (empty vector) for 4 h. Cells were lysed and the binding of the different CNF_Y proteins to HEp-2 cells was analyzed by immunoblotting.

B HEp-2 cells were incubated with 20 µg/ml of whole cell extract of *Y. pseudotuberculosis* expressing CNF_Y, the toxin variant mut1: CNF_YI535L/P536A/V537G or mut2: CNF_YI535L/P536A/V537G/F539L/D541A/K542A or no CNF_Y protein (empty vector). The cell nuclei were stained with DAPI (blue) and the actin cytoskeleton was stained using FITC-phalloidin (green). The results indicated the formation of polynucleated cells and stress fibers only in cells treated with CNF_Y and CNF_YI535L/P536/V537G. The white scale bar is 20 µm.

C Nitrocefin (2 mM) was added to the supernatant from 25°C overnight *Yersinia* cultures expressing the indicated CNF_Y derivatives to determine β-lactamase activity by measuring changes in absorbance at 390 nm (yellow) and 486 nm (red).

D The viability of *Y. pseudotuberculosis* YPIII expressing the indicated CNF_Y derivatives was assessed in equalized bacterial cultures using the BacTiter-Glo Microbial Cell Viability Assay kit (Promega).

E HEp-2 cells treated with 20 µg/ml of whole cell extract of *Y. pseudotuberculosis* expressing indicated CNF_Y variants for 4 h were lysed and the deamidation of RhoA was analyzed by the mobility shift of the modified RhoA GTPase detected by immunoblotting.

F The activity of the CNF_Y derivatives was tested by analyzing the deamidation of RhoA in HEp-2 cell lysates by the mobility shift of the modified GTPase detected by immunoblotting.

Figure 7. Structure and deamidation activity of the free D4-5 subunit of CNF_Y.

A Crystal structure of the free D4-5 subunit. Note the different relative orientations of domains D4 and D5 with respect to the structure of full-length CNF_Y (top, thin grey lines). The domain D4 forms a large interface area (1100 $Å^2$) with the catalytic domain D5 involving several polar interactions (8 hydrogen bonds and 8 salt bridges), whereby the active crevice is extended and fully solvent-exposed as can be seen in the right surface plot at the bottom of the panel. The hypothetical NAD^+ binding site of the ART-like D4 domain is located on the opposite face (left surface plot). Note that the deamidase active site of domain D5, unlike in the full-length structure (Fig 1), is fully accessible and that its extended shape is also determined by domain D4.

B Comparative analysis of RhoA activation in HEp-2 cell lysate by CNF_Y and the recombinant D4-5 protein. Purified CNF_Y or the D4-5 fragment (1 µM) was added to extracts of HEp-2 cells and incubated for 10, 20, 30 or 60 min. Deamidation of RhoA was analyzed by the shift of the modified Rho GTPase band in SDS PAGE gels after detection with anti-RhoA antibodies.

C Comparative analysis of recombinant RhoA deamidation by CNF_Y and the D4-5 fragment. Recombinant RhoA was incubated with purified CNF_Y or the D4-5 fragment and samples were separated by SDS-PAGE after the indicated times before subjecting to trypsin digestion and quantification of deamidation of Q63 by mass spectrometry. Error bars represent standard deviations of triplicate measurements.

Figure 8. Architecture of bacterial toxins with a CNF-like translocation apparatus

Shown are the architecture of CNF_Y, *Pasteurella multocida* toxin PMT and two uncharacterized proteins from *Pseudomonas syringiae*. The released fragment of PMT contains three domains of which C1 is required for membrane binding, the C2 domain has an unknown function and the C3-domain activates heterotrimeric G-proteins by deamidation. The two *Pseudomonas syringiae* proteins A0A0P9UH04 and A0A0N8SZE6

represent two uncharacterized toxins that encode catalytic domains of the indicated type. While sequence alignments unequivocally reveal a CNF-like imperfect β-barrel in PMT, the presence of this domain in the *P. syringiae* toxins is less obvious.

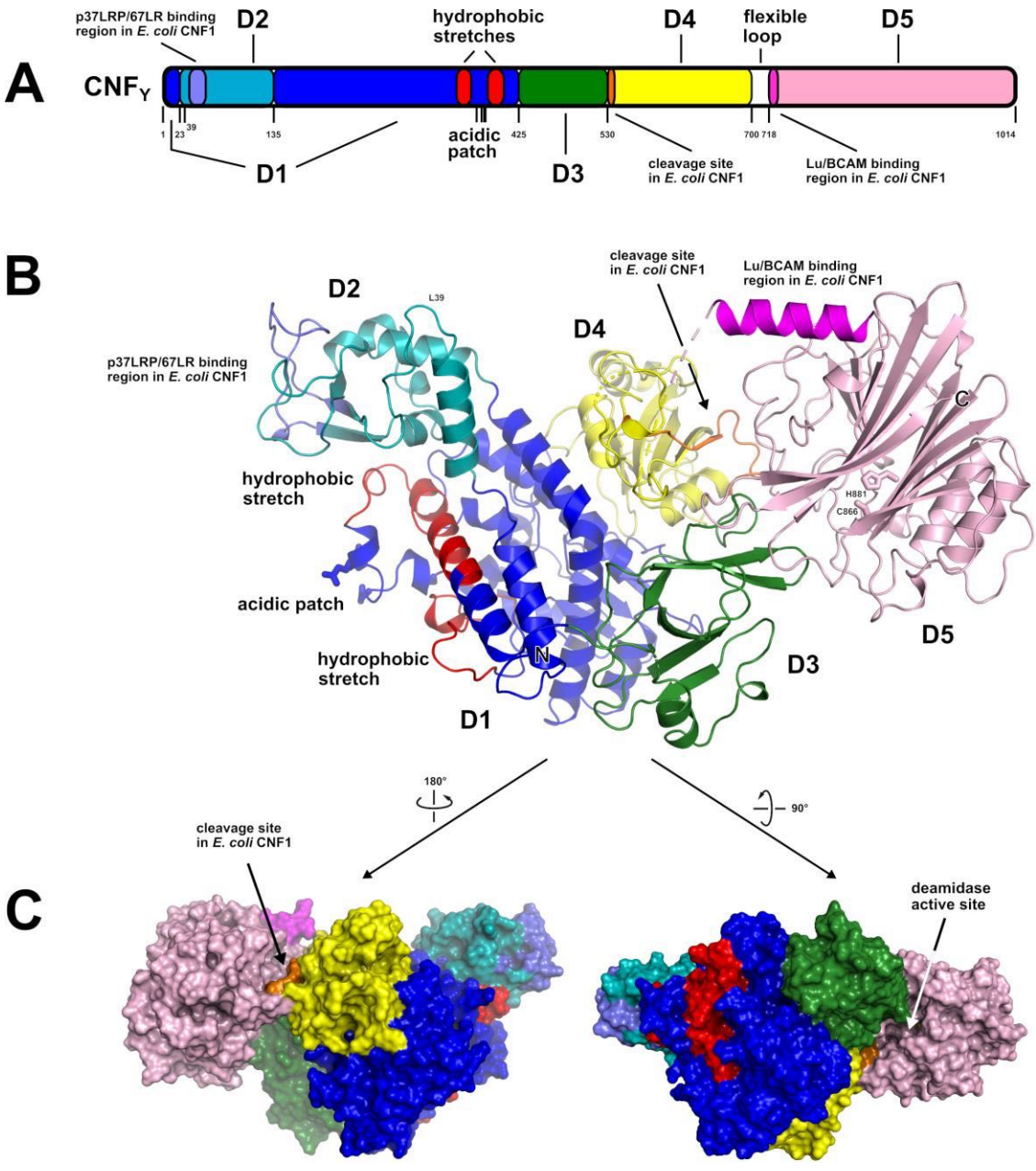
A
p37LRP/67LR binding region in E. coli CNF1
D2
hydrophobic stretches
D4
flexible loop
D5
CNFY
1
23
39
135
acidic patch
425
530
700 718
1014
D1
D3
cleavage site in E. coli CNF1
Lu/BCAM binding region in E. coli CNF1
B
D2
L39
cleavage site in E. coli CNF1
Lu/BCAM binding region in E. coli CNF1
D4
p37LRP/67LR binding region in E. coli CNF1
C
hydrophobic stretch
H881
C866
acidic patch
N
hydrophobic stretch
D5
D3
D1
C
180°
90°
cleavage site in E. coli CNF1
deamidase active site

Figure 1

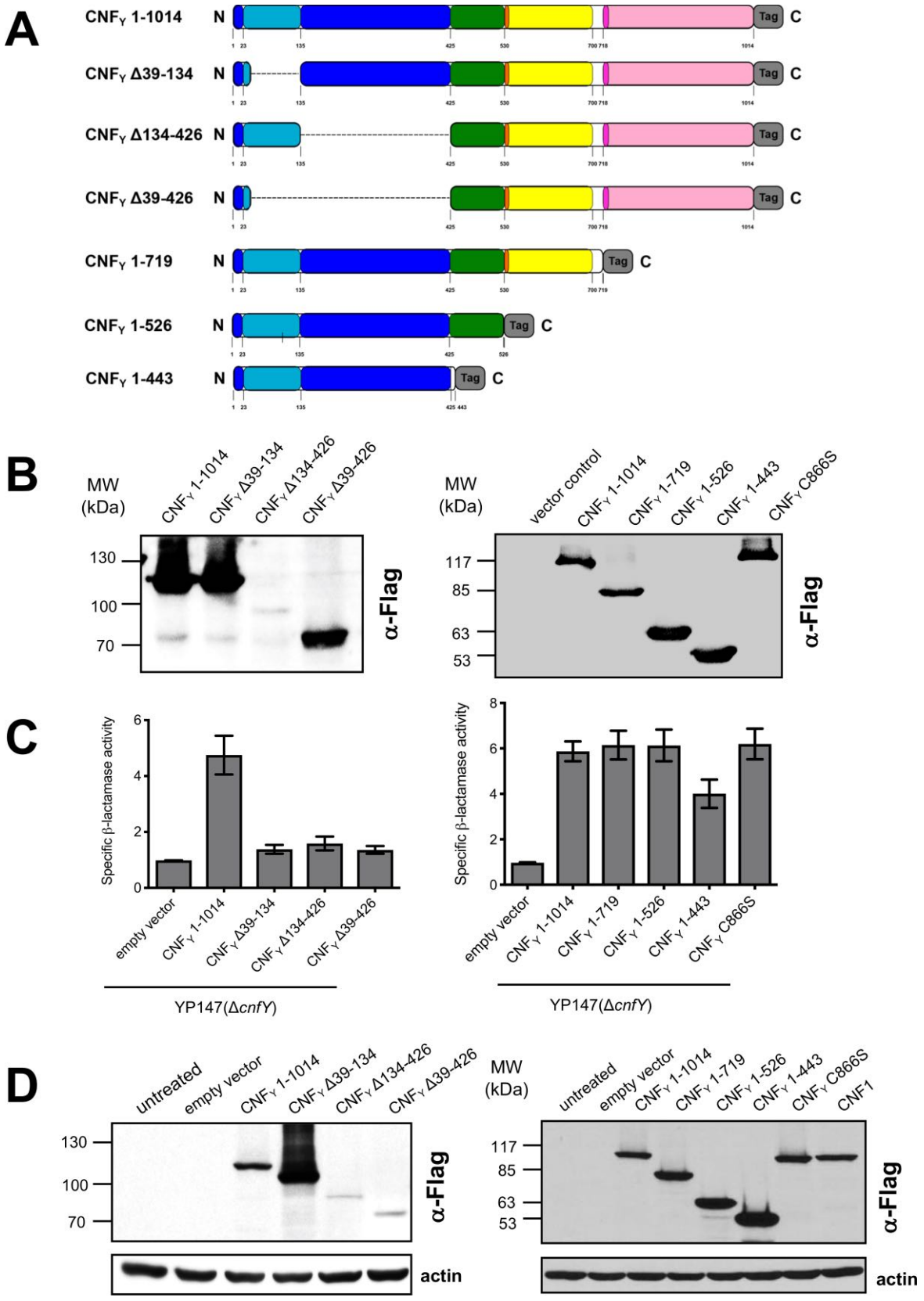
A
CNFγ 1-1014
CNFγ Δ39-134
CNFγ Δ134-426
CNFγ Δ39-426
CNFγ 1-719
CNFγ 1-526
CNFγ 1-443
N
C
Tag
B
MW (kDa)
CNFγ 1-1014
CNFγ Δ39-134
CNFγ Δ134-426
CNFγ Δ39-426
130
100
70
α-Flag
vector control
CNFγ 1-1014
CNFγ 1-719
CNFγ 1-526
CNFγ 1-443
CNFγ C866S
117
85
63
53
α-Flag
C
Specific β-lactamase activity
empty vector
CNFγ 1-1014
CNFγ Δ39-134
CNFγ Δ134-426
CNFγ Δ39-426
YP147(ΔcnfY)
CNFγ 1-719
CNFγ 1-526
CNFγ 1-443
CNFγ C866S
D
untreated
empty vector
CNFγ 1-1014
CNFγ Δ39-134
CNFγ Δ134-426
CNFγ Δ39-426
MW (kDa)
CNFγ 1-719
CNFγ 1-526
CNFγ 1-443
CNFγ C866S
CNF1
α-Flag
actin

Figure 2

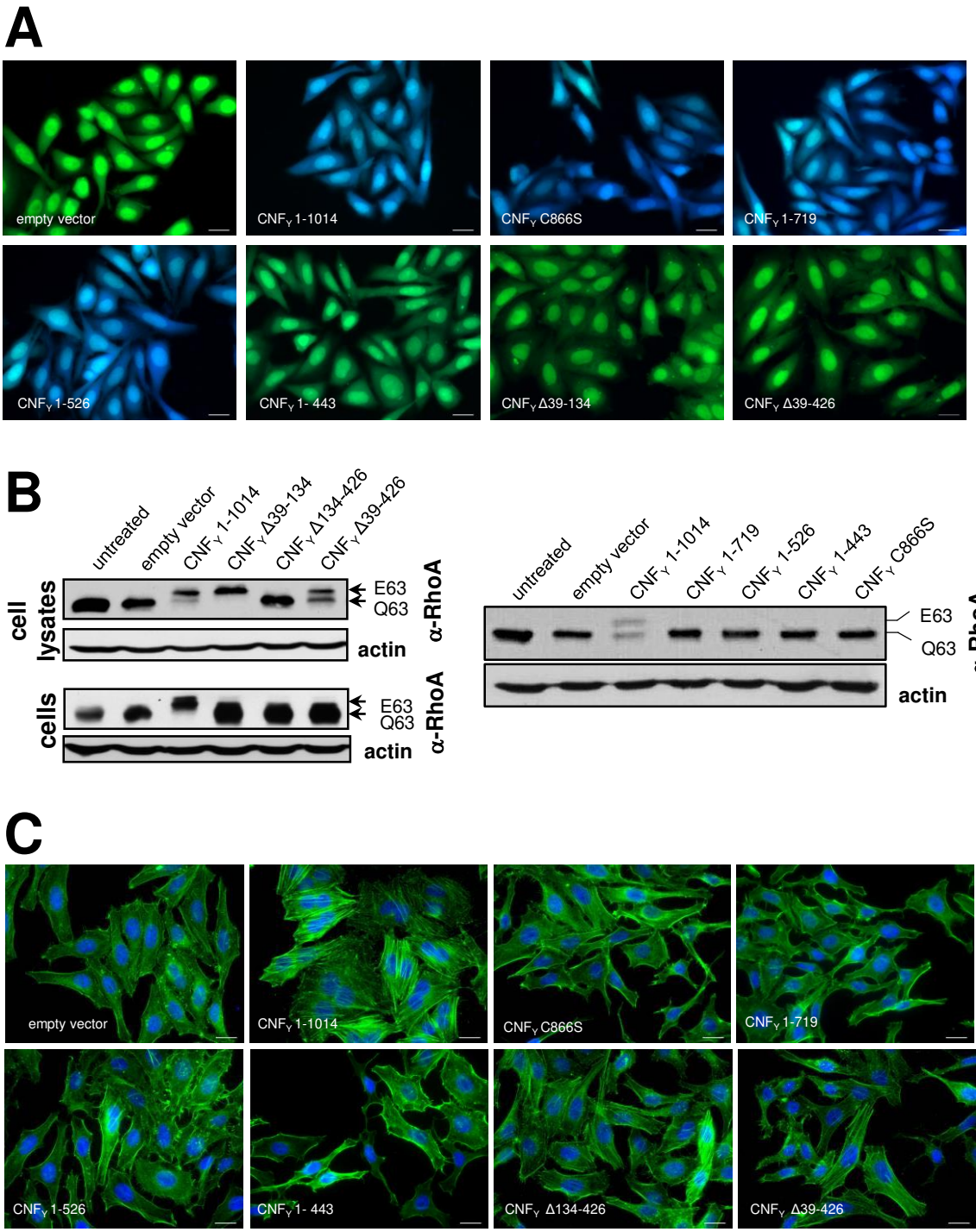
A
empty vector
CNFγ 1-1014
CNFγ C866S
CNFγ 1-719
CNFγ 1-526
CNFγ 1- 443
CNFγ Δ39-134
CNFγ Δ39-426
B
untreated
empty vector
CNFγ 1-1014
CNFγ Δ39-134
CNFγ Δ134-426
CNFγ Δ39-426
cell lysates
E63
Q63
α-RhoA
actin
cells
E63
Q63
α-RhoA
actin
untreated
empty vector
CNFγ 1-1014
CNFγ 1-719
CNFγ 1-526
CNFγ 1-443
CNFγ C866S
E63
Q63
α-RhoA
actin
C
empty vector
CNFγ 1-1014
CNFγ C866S
CNFγ 1-719
CNFγ 1-526
CNFγ 1- 443
CNFγ Δ134-426
CNFγ Δ39-426

Figure 3

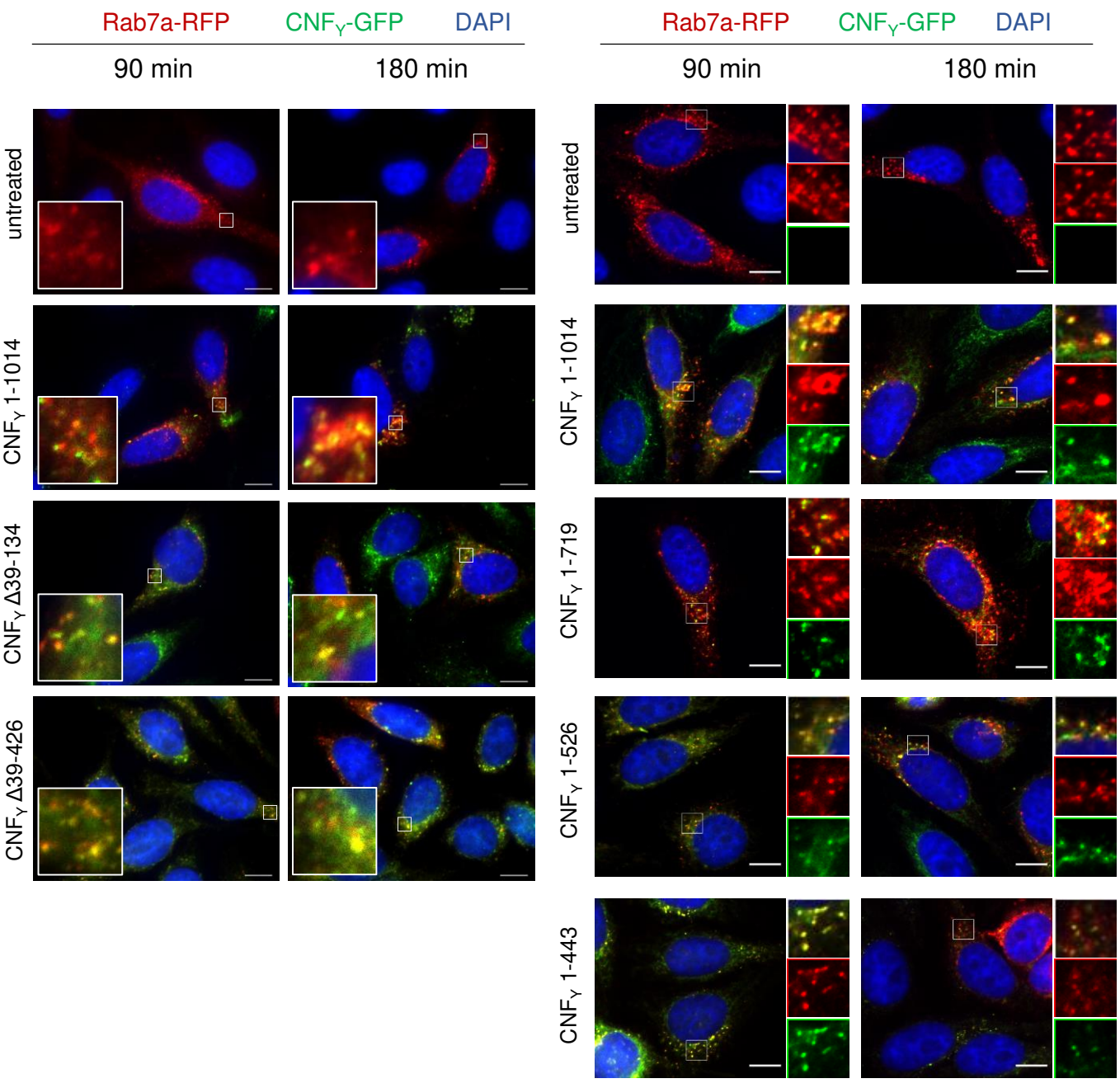
Rab7a-RFP
CNFY-GFP
DAPI
90 min
180 min
untreated
CNFY 1-1014
CNFY Δ39-134
CNFY Δ39-426
CNFY 1-719
CNFY 1-526
CNFY 1-443

Figure 4

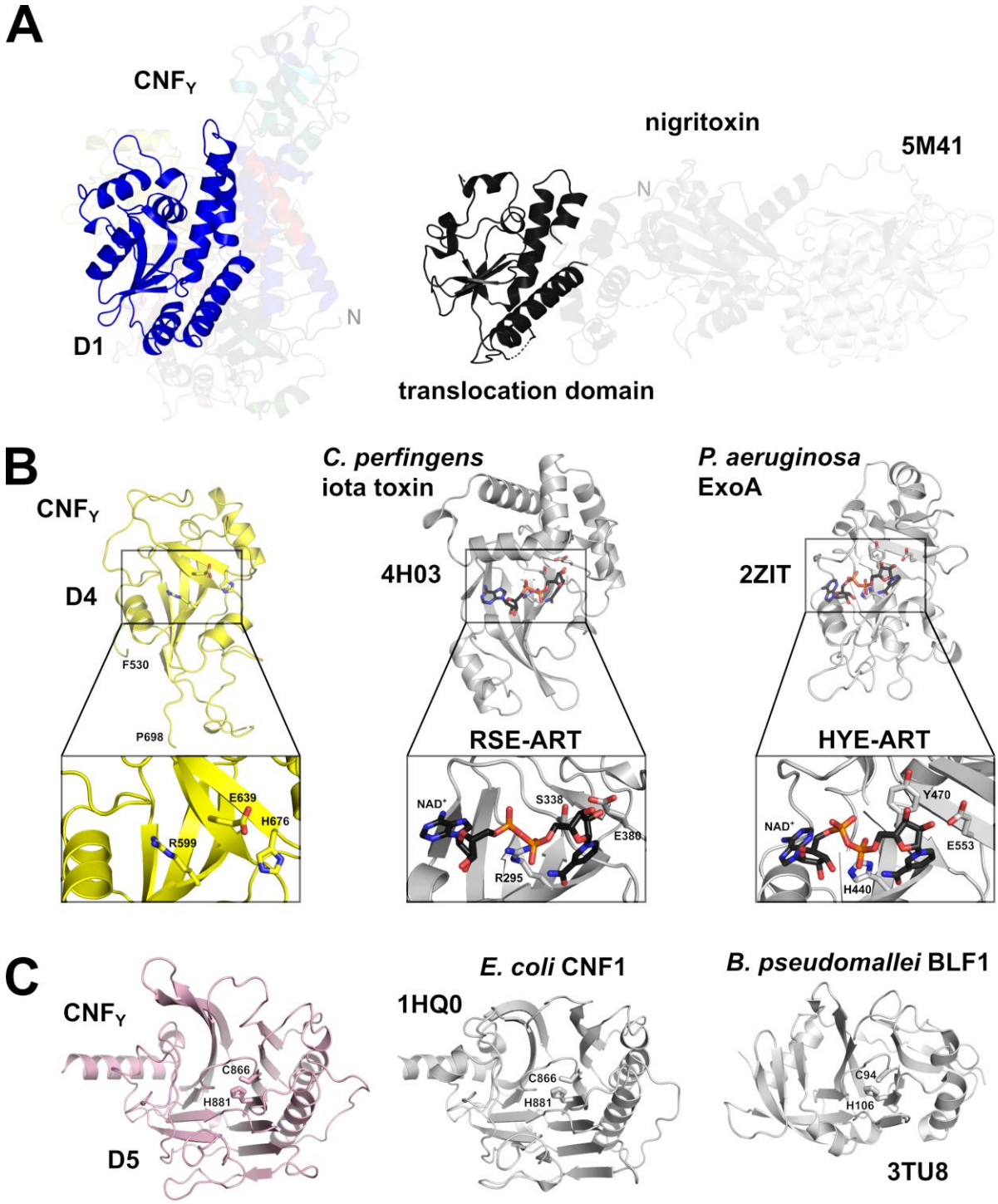
A
CNFY
D1
N
nigritoxin
5M41
N
translocation domain
B
CNFY
D4
F530
P698
E639
H676
R599
C. perfingens
iota toxin
4H03
RSE-ART
NAD+
S338
E380
R295
P. aeruginosa
ExoA
2ZIT
HYE-ART
Y470
NAD+
E553
H440
C
CNFY
C866
H881
D5
E. coli CNF1
1HQ0
C866
H881
B. pseudomallei BLF1
C94
H106
3TU8

Figure 5

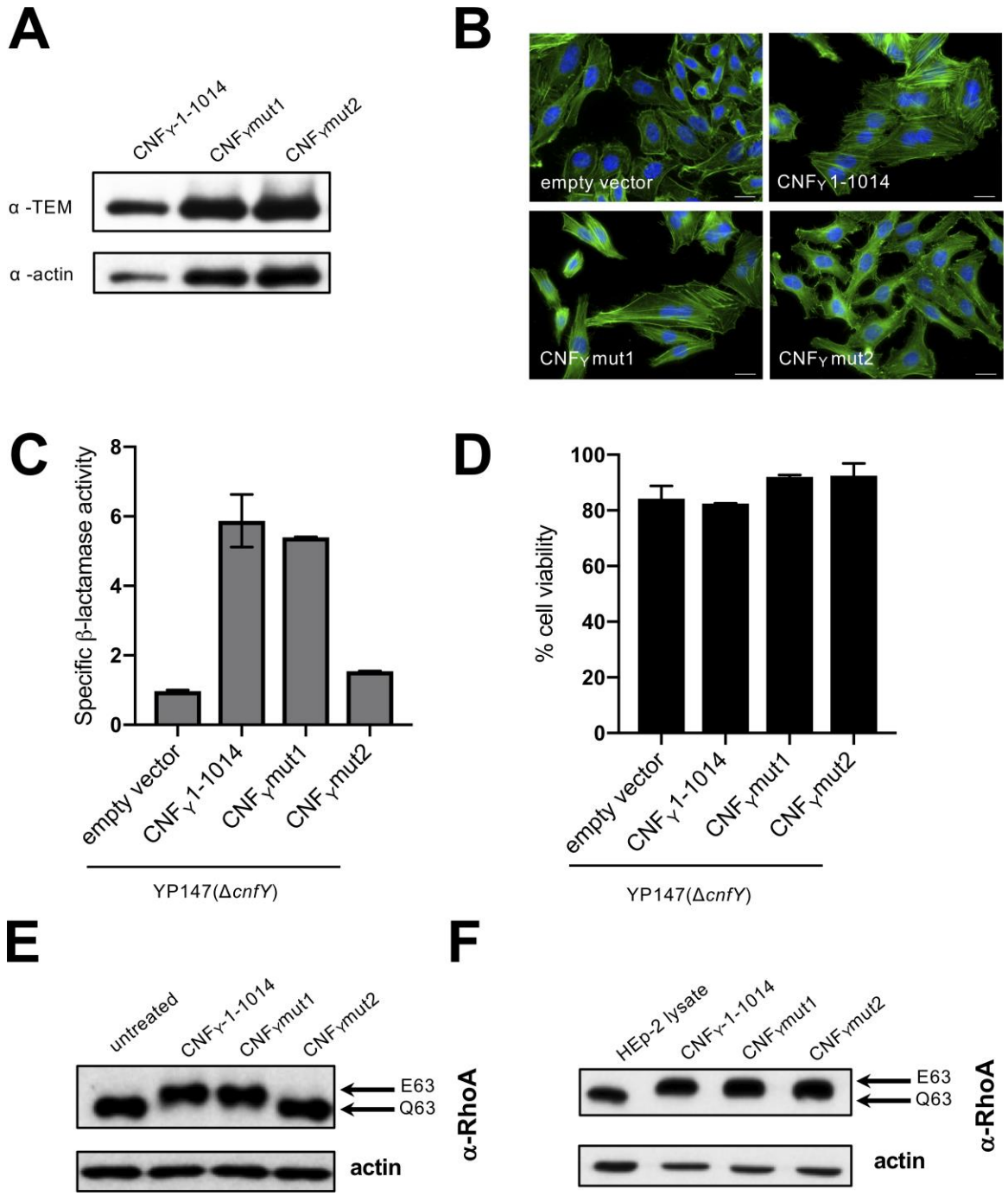
A
CNFγ-1-1014
CNFγmut1
CNFγmut2
α -TEM
α -actin
B
empty vector
CNFγ1-1014
CNFγmut1
CNFγmut2
C
Specific β-lactamase activity
0
2
4
6
8
empty vector
CNFγ1-1014
CNFγmut1
CNFγmut2
YP147(ΔcnfY)
D
% cell viability
0
20
40
60
80
100
empty vector
CNFγ1-1014
CNFγmut1
CNFγmut2
YP147(ΔcnfY)
E
untreated
CNFγ-1-1014
CNFγmut1
CNFγmut2
E63
Q63
actin
α-RhoA
F
HEp-2 lysate
CNFγ-1-1014
CNFγmut1
CNFγmut2
E63
Q63
actin
α-RhoA

Figure 6

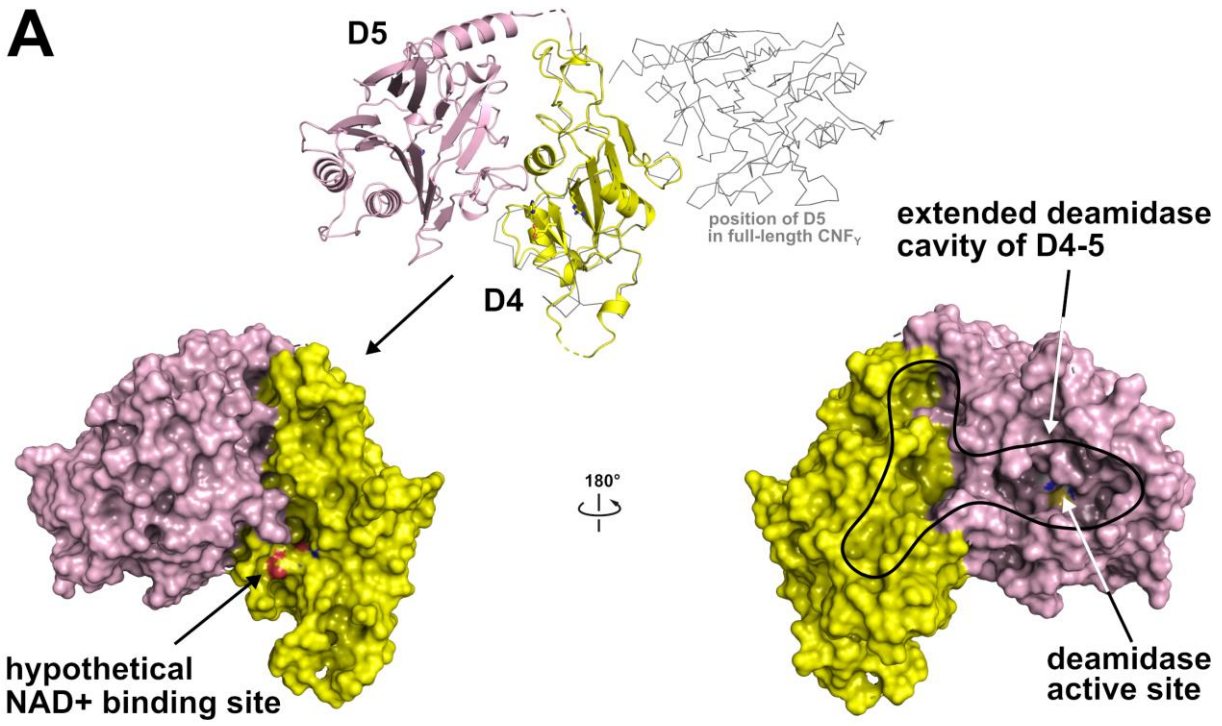
A
D5
D4
position of D5
in full-length CNFY
extended deamidase
cavity of D4-5
180°
hypothetical
NAD+ binding site
deamidase
active site

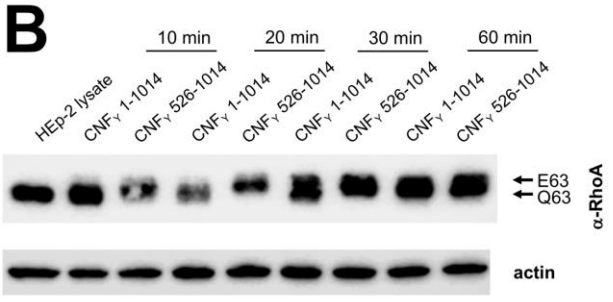
B
10 min
20 min
30 min
60 min
HEp-2 lysate
CNFY 1-1014
CNFY 526-1014
E63
Q63
α-RhoA
actin

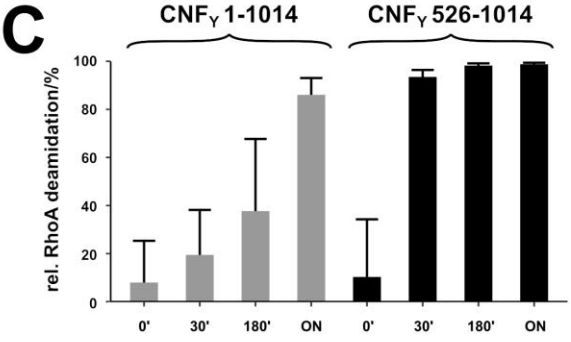
C
CNFY 1-1014
CNFY 526-1014
rel. RhoA deamidation/%
0
20
40
60
80
100
0'
30'
180'
ON

Figure 7

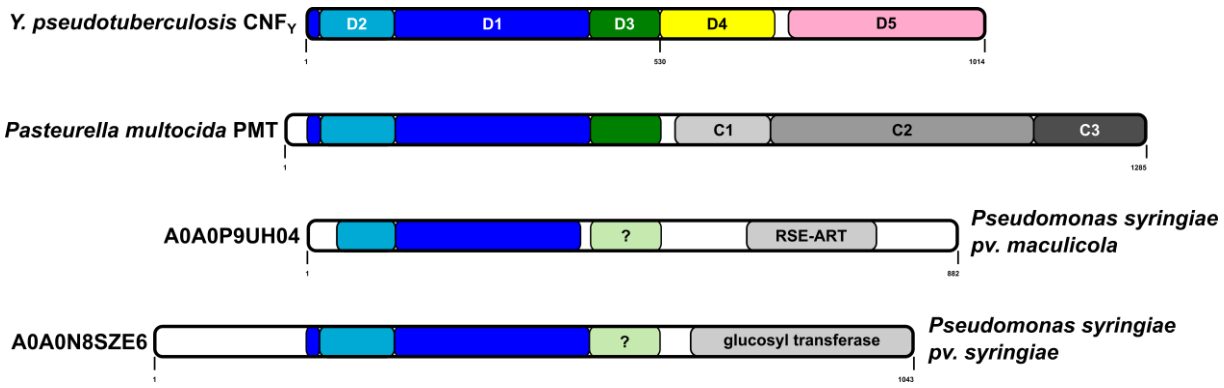
Y. pseudotuberculosis CNFY
D2
D1
D3
D4
D5
1
530
1014
Pasteurella multocida PMT
C1
C2
C3
1
1285
A0A0P9UH04
?
RSE-ART
1
882
Pseudomonas syringiae
pv. maculicola
A0A0N8SZE6
?
glucosyl transferase
1
1043
Pseudomonas syringiae
pv. syringiae

Figure 8

Expanded View Tables

Table EV1. X-ray data collection and refinement statistics.

Structure	CNF_Y 1-704 SeMet	CNF_Y 1-704 nat	CNF_Y 720-1014	CNF_Y 526-1014	CNF_Y full-length (C866S)
PDB-ID:	**-**	**6Q7Z**	**6Q7Y**	**6Q80**	**6Q7X**
Data collection					
Beamline	BESSY BL 14.1	SLS X06DA (PXIII)	BESSY BL 14.2	SLS X06DA (PXIII)	SLS X06DA (PXIII)
Wavelength (Å)	0.98	1.00	0.92	1.00	1.00
Space group	$P2_1$	$P2_1$	$P2_1$	$P2_12_12_1$	$I2_12_12_1$
Cell dimensions					
a, *b*, *c* (Å)	94.26, 99.70, 131.06	94.43, 99.90, 131.36	41.98, 50.16, 69.73	48.27, 90.53, 120.72	70.15, 180.42, 220.76
α, β, γ (°)	90.00, 95.85, 90.00	90.00, 95.86, 90.00	90.00, 98.72, 90.00	90.00, 90.00, 90.00	90.00, 90.00, 90.00
Resolution (Å)[a]	49.01 – 3.8 (4.06– 3.8)	99.90 - 3.28 (3.33 - 3.28)	68.92 - 1.14 (1.15 - 1.14)	48.27 – 1.80 (1.84 – 1.80)	47.08 - 2.70 (2.82 – 2.70)
R_{merge} (%)[a]	21.3 (68.9)	8.8 (90.1)	3.6 (43.8)	25.7 (350.6)	10.6 (180.5)
R_{pim} (%)[a]	5.9 (18.7)	3.6 (36.2)	2.4 (29.5)	4.6 (81.5)	2.3 (39.2)
$I/\sigma I$[a]	13.0 (4.7)	17.8 (2.2)	16.0 (2.2)	12.4 (1.6)	23.3 (2.2)
Completeness (%)[a]	100.0 (100.0)	99.9 (100.0)	95.2 (99.7)	99.9 (98.6)	99.9 (99.5)
Redundancy[a]	13.8 (14.5) anomalous: 7.0 (7.3)	6.9 (7.1)	3.0 (2.9)	32.7 (19.8)	21.4 (22.0)
$CC_{1/2}$ (%)[a]	99.7 (93.6)	99.9 (77.4)	99.9 (88.2)	98.2 (81.6)	100 (76.1)
Refinement					
Resolution (Å)	3.8	3.28	1.14	1.80	2.70
No. reflections	24050	37535	100644	49821	38988
R_{work}/ R_{free} (%)		24.05/26.46	16.74/18.22	15.81/19.10	20.48/24.19
No. atoms		12248	3084	4532	8847
Protein		12248	2745	4147	8745
Ligand/ion		0	1	18	46
Water		0	338	367	56
B-factors ($Å^2$)		95.89	19.59	35.07	86.94
Protein		95.89	18.65	34.28	86.99
Ligand/ion		-	21.19	70.13	101.15
Water		-	27.21	42.28	67.60
R.m.s deviations					
Bond lengths (Å)		0.003	0.010	0.004	0.03
Bond angles (º)		0.608	1.123	0.676	0.578
Ramachandran statistics (%)					
Favored		95.10	97.23	97.76	96.35
Allowed		4.39	2.77	2.24	3.65
Outliers		0.50	0.00	0.00	0.00

[a]Values for the highest resolution shell are shown in parentheses.

Expanded View Figures

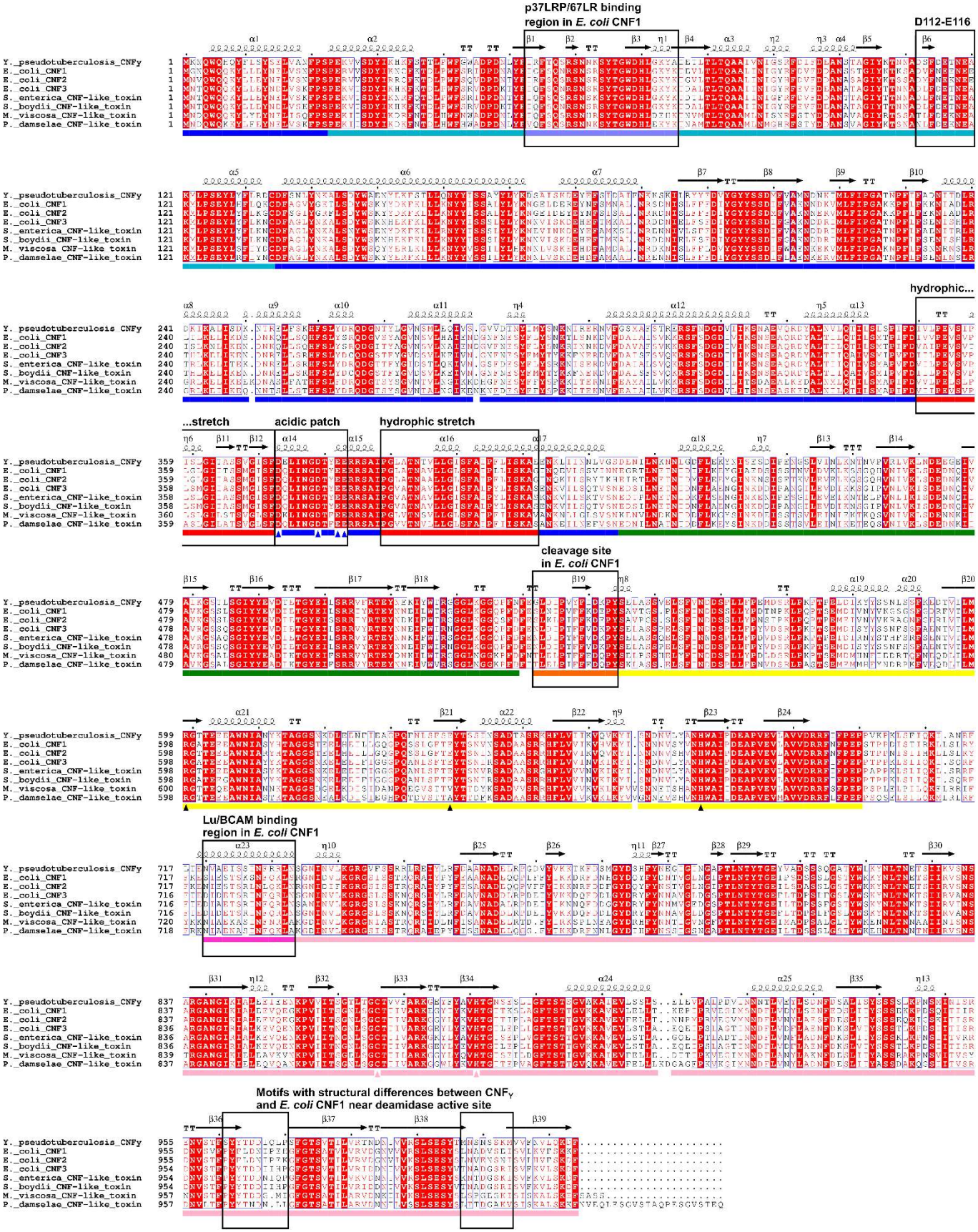

Figure EV1. Sequence alignment of CNF_Y to other CNFs.

Sequences from top to bottom: 1. CNF_Y from *Yersinia pseudotuberculosis*, 2. CNF1 from *E. coli* (NCBI accession: AAA85196, 61% sequence identity to CNF_Y), 3. CNF2 from *E. coli* (NCBI accession: ACT33566, 61% sequence identity), 4. CNF3 from *E. coli* (NCBI accession: CAK19001, 68% sequence identity), 5. CNF from *Salmonella enterica* (NCBI accession: WP_079946821, 69% sequence identity), 6. CNF from *Shigella boydii* (NCBI accession: WP_075330563, 68% sequence identity), 7. CNF from *Moritella viscosa* (NCBI accession: AHI58923, 58% sequence identity). 8. CNF from *Photobacterium damselae* (NCBI accession: WP_005306733, 58% sequence identity).
Columns with identical residues are highlighted in red. The sequence alignment was generated using ClustalX (Larkin, Blackshields et al., 2007) and formatted using the ESPript 3 webservice (Robert & Gouet, 2014). The alignment has been annotated with the secondary structure extracted from the structural model of full-length CNF_Y. The domains of CNF_Y are indicated below the sequences using the coloring scheme used in Fig. 1. Specific residues that are supposed to be functionally relevant are marked by arrows in the domain annotation.

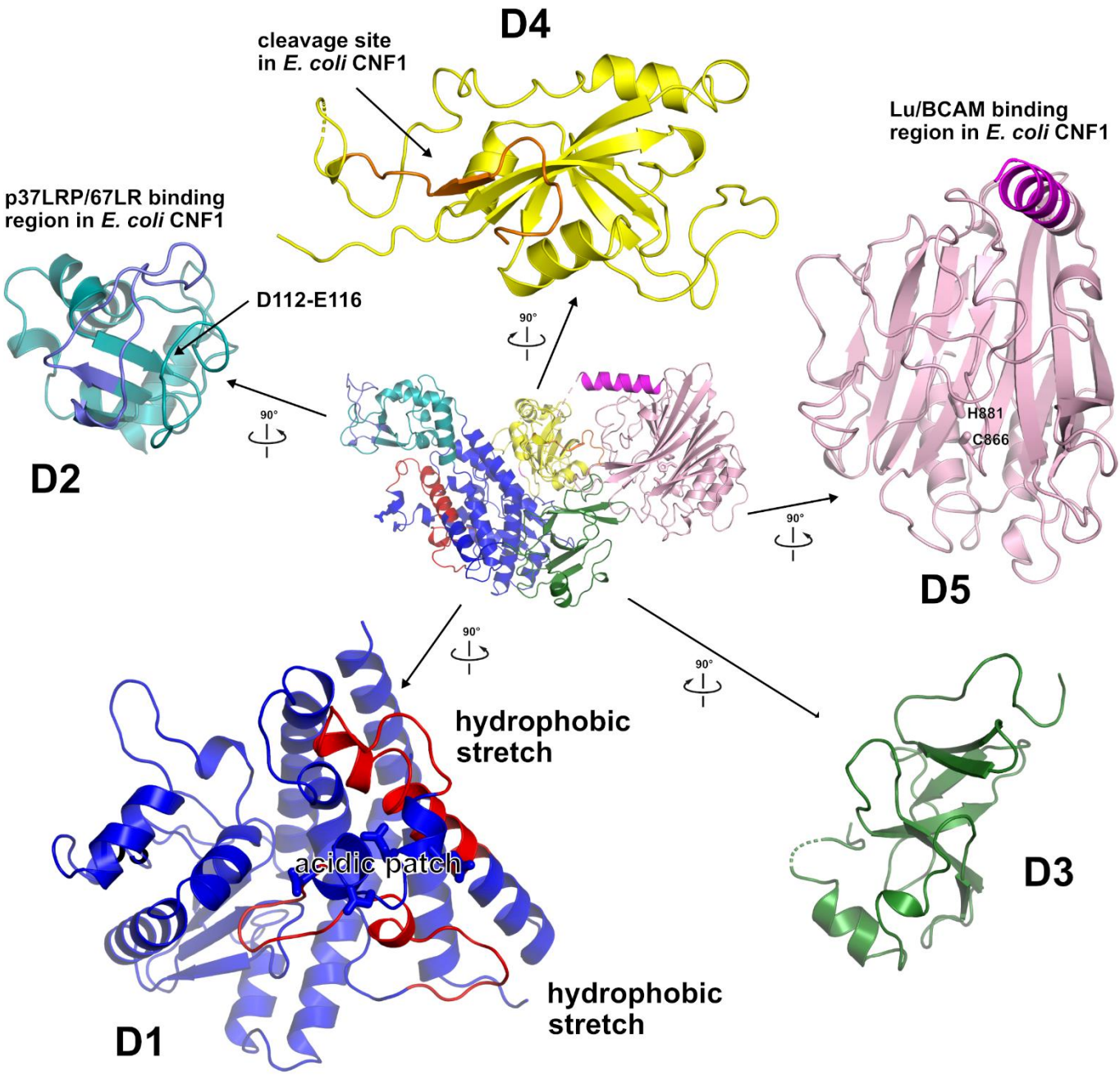

Figure EV2. Exploded view of CNF_Y.

Cartoon representation of full-length CNF_Y (middle) surrounded by enlarged perpendicular views of the individual domains D1 to D5, colored according to domain boundaries determined with PiSQRD (Aleksiev *et al*, 2009). Dark blue: domain D1, cyan: domain D2, dark green: domain D3, yellow: ADP-ribosyltransferase-like domain D4, pink: deamidase domain D5. Other colors indicate the position of sequence motifs that have been identified in *E. coli* CNF1, namely light purple: p37LRP/67LR receptor-binding motif, red: hydrophobic stretches predicted to form membrane-inserting α-helices, orange: cleavage site, magenta: main Lu/BCAM receptor-binding motif.

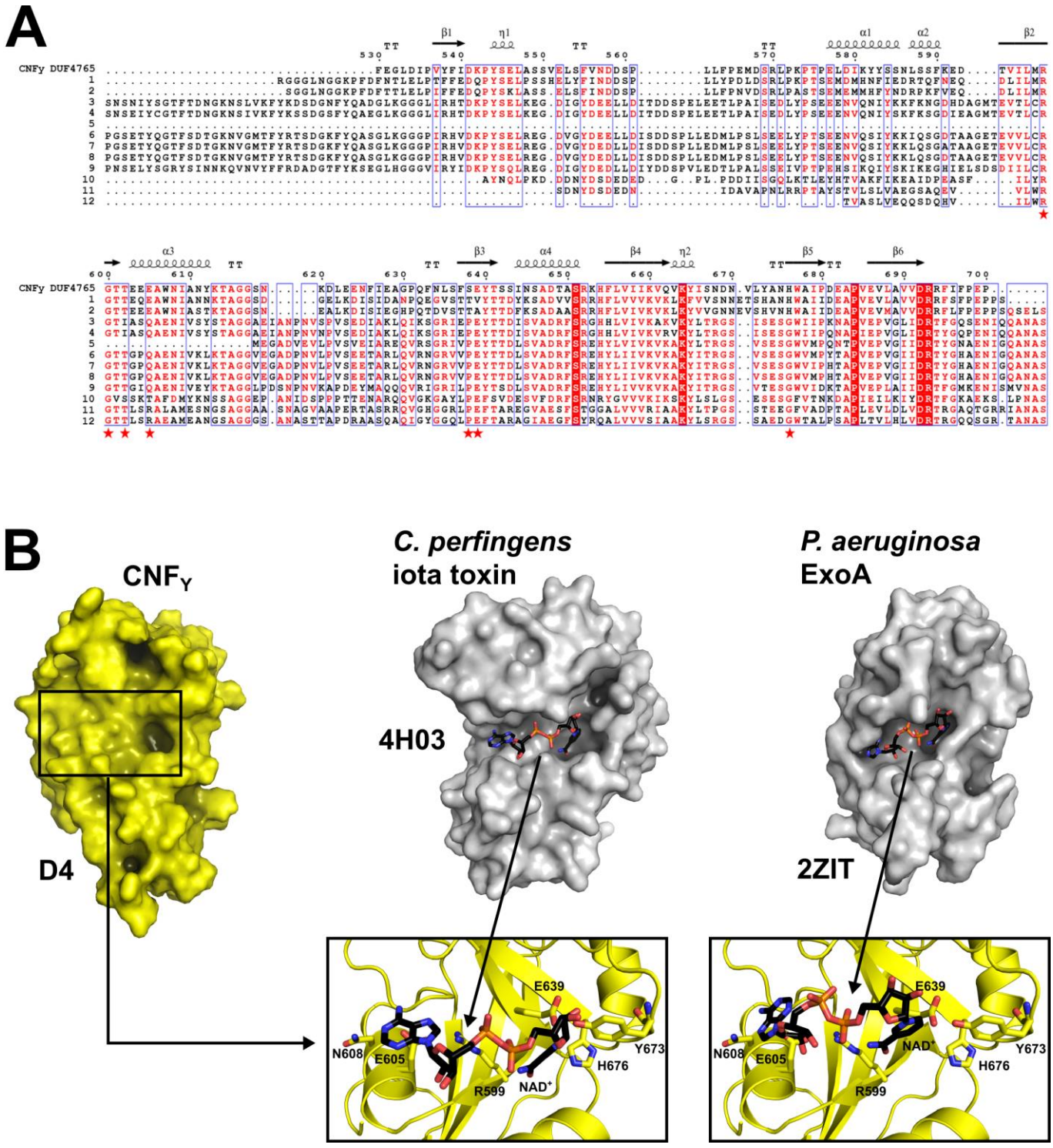

Figure EV3. Exploded view of CNF_Y.

Cartoon representation of full-length CNF_Y (middle) surrounded by enlarged perpendicular views of the individual domains D1 to D5, colored according to domain boundaries determined with PiSQRD (Aleksiev *et al*, 2009). Dark blue: domain D1, cyan: domain D2, dark green: domain D3, yellow: ADP-ribosyltransferase-like domain D4, pink: deamidase domain D5. Other colors indicate the position of sequence motifs that have been identified in *E. coli* CNF1, namely light purple: p37LRP/67LR receptor-binding motif, red: hydrophobic stretches predicted to form membrane-inserting α-helices, orange: cleavage site, magenta: main Lu/BCAM receptor-binding motif.

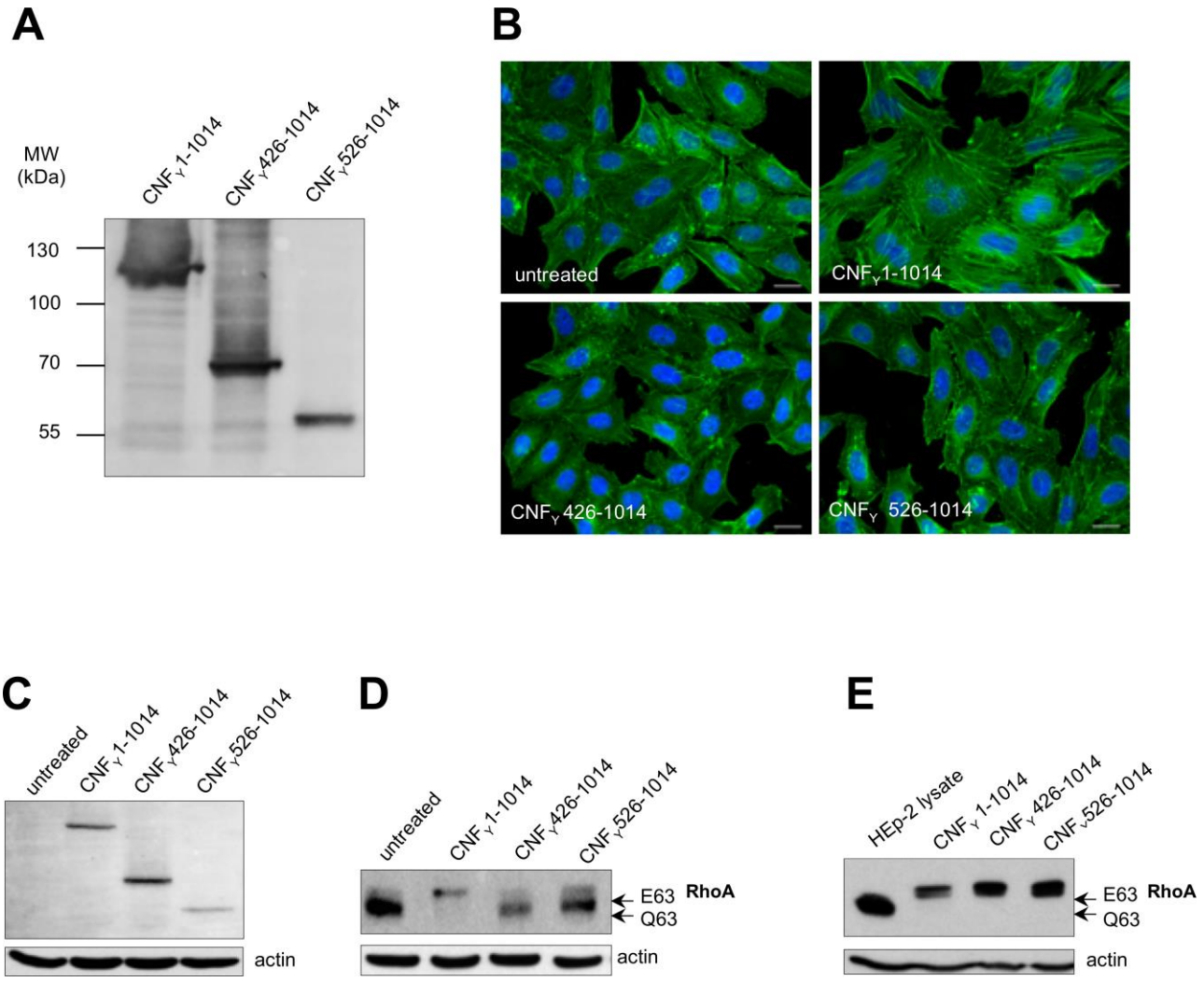

Figure EV4. C-terminal domain D3-5 and D4-5 are able to bind to host cells and deaminate RhoA.

A The expression of purified recombinant CNF_Y N-terminal domains D3-5 (CNF_Y 426-1014) or D4-5 (CNF_Y 526-1014).

B HEp-2 cells remain untreated or were incubated with 500 nM purified full-length CNF_Y, domains D3-5 (CNF_Y 426-1014) or D4-5 (CNF_Y 526-1014) for 24 h. The formation of large, multinuclear cells was observed by fluorescence microscopy. The cell nuclei were strained with DAPI (blue) and the actin cytoskeleton was stained using FITC-Phalloidin (green). The white scale bar is 20 µm.

C Binding of purified full-length CNF_Y, domains D3-5 (CNF_Y 426-1014) or D4-5 (CNF_Y 526-1014) to HEp-2 cells was analyzed by immunoblotting after HEp-2 cells were incubated with 500 nM of the purified toxin or toxin fragments for 4 h.

D HEp-2 cells treated with 500 nM purified full-length CNF_Y, protein fragments D3-5 (CNF_Y 426-1014) or D4-5 (CNF_Y 526-1014) were lysed and the deamidation of RhoA was analyzed by the mobility shift of the modified GTPase detected by immunoblotting.

E The activity of purified CNF_Y and the protein fragments D3-5 (CNF_Y 426-1014) or D4-5 (CNF_Y 526-1014) was tested by analyzing the deamidation of RhoA in HEp-2 cell lysates by the mobility shift of the modified GTPase detected by immunoblotting.

Appendix tables and figures

Index

Appendix Tables

Table S1. Domain Interfaces.

The CNF_Y structural model was split at the domain boundaries and surfaces of the isolated domains and domain-domain interface areas were calculated using PDBe PISA (Krissinel & Henrick, 2007).

Domain	**1-425**	**426-526**	**527-700**	**718-1014**
Surface area	19224 Å^2	5858 Å^2	9853 Å^2	12864 Å^2
1-425	-	756 Å^2	1428 Å^2	no contact
426-526	756 Å^2	-	438 Å^2	611 Å^2
527-700	1428 Å^2	438 Å^2	-	385 Å^2
719-1014	no contact	611 Å^2	385 Å^2	-

Table S2. Structural homology of domain D4.

Structures with folds similar to domain D4 of CNF_Y as identified by DALI (Holm & Rosenstrom, 2010). Listed below are the 10 highest scoring results, ordered according to their Z-score in descending order.

PDB entry	**Chain**	**Z-score**	**C_α R.m.s.d. (Å)**	**length of alignment**	**number of residues in target**	**% sequence-identity**	**Description**
5LYH	A	5.6	3.6	101	185	11	Human poly(ADP-ribose) polymerase 14
1WFX	A	5.5	2.9	78	180	19	2'-phosphotransferase from *Aeropyrum pernix*
3HKV	A	5.3	4.0	102	192	9	Human poly(ADP-ribose) polymerase 10
4F0D	A	5.2	3.8	103	238	12	Human poly(ADP-ribose) polymerase 16
2Q5T	A	5.2	4.1	100	605	11	Cholix toxin from *Vibrio cholerae*
2AUA	B	4.7	3.0	72	210	13	Protein of unknown function from *Bacillus cereus*
1DDT	A	4.7	3.6	94	523	12	Diphteria toxin from *Corynebacterium diphtheriae*
4HYF	A	4.5	4.7	101	227	10	Human tankyrase-2
4TLV	A	4.4	4.9	89	582	11	CARDS toxin from *Mycoplasma pneumoniae*
3AQ2	A	4.4	3.1	96	191	10	Protein 6b from *Agrobacterium vitis*

Table S3: Strains and plasmids.

Strain	Characteristics	Source/Reference
YPIII	Wild type *Yersinia pseudotuberculosis* serogroup III	(Bolin, Norlander et al., 1982)
YP147	YPIII, Δ*cnfY*::Kn^R	(Schweer, Kulkarni et al., 2013)
DH10β		Invitrogen
Rosetta II (DE3)		Novagen
BL21 (DE3)		Novagen
Plasmid		
pFU189	Cm^R	(Uliczka & Dersch, 2012)
pTEM	Cm^R	this study
pCNF$_Y$-TEM	Cm^R	this study
pCNF$_{YC866S}$-TEM	Cm^R	this study
pCNF$_{Y1-719}$-TEM	Cm^R	this study
pCNF$_{Y1-526}$-TEM	Cm^R	this study
pCNF$_{Y1-443}$-TEM	Cm^R	this study
pCNF$_{YΔ39-134}$-TEM	Cm^R	this study
pCNF$_{YΔ134-426}$-TEM	Cm^R	this study
pCNF$_{YΔ39-426}$-TEM	Cm^R	this study
pCNF$_{YΔ527-719}$-TEM	Cm^R	this study
pCNF$_{YΔ527-699}$-TEM	Cm^R	this study
pCNF$_{YE382/383K}$-TEM	Cm^R	this study
p3xFLAG	Cm^R	this study
pCNF$_Y$-3xFLAG	Cm^R	this study
pCNF$_{YC866S}$-3xFLAG	Cm^R	this study
pCNF$_{Y1-719}$-3xFLAG	Cm^R	this study
pCNF$_{Y1-526}$-3xFLAG	Cm^R	this study
pCNF$_{Y1-443}$-3xFLAG	Cm^R	this study
pCNF$_{YΔ39-134}$-3xFLAG	Cm^R	this study
pCNF$_{YΔ134-426}$-3xFLAG	Cm^R	this study
pCNF$_{YΔ39-426}$-3xFLAG	Cm^R	this study
pCNF$_{YΔ527-719}$-3xFLAG	Cm^R	this study
pCNF$_{YΔ527-699}$-3xFLAG	Cm^R	this study
pCNF$_{YE382/383K}$-3xFLAG	Cm^R	this study
pCNF$_{Y\ I535L/P536A/V537G}$-TEM	Cm^R	this study
pCNF$_{YI535L/P536A/V537G/F539L/D541A/K542A}$-TEM	Cm^R	this study
pCNF$_Y$-GFP	Cm^R	this study
pCNF$_{Y1-719}$-GFP	Cm^R	this study
pCNF$_{Y1-526}$-GFP	Cm^R	this study
pCNF$_{Y1-443}$-GFP	Cm^R	this study
pCOLA-Duet-1	Kan^R	Novagen
pET28c-CNF$_Y$1-704	Kan^R - construct for crystallography purposes	this study
pET28c-CNF$_Y$720-1014	Kan^R - construct for crystallography purposes	this study
pVP-CNF$_Y$526-1014-3xFlag	Kan^R - construct for crystallography purposes	this study
pVP-CNF$_Y$FL-C866S	Kan^R - construct for crystallography purposes	this study

Table S4: Oligonucleotide primers.

Primer	Sequence 5' – 3'	
blaM F	GGCCTGCAGGCCACCCAGAAACGCTGGTGAA	*blaM* cloning into pFU189 *Pst*I
blaM R	GTTGCGGCCGCTTTACCAATGCTTAATCAGTGAGGCA	*blaM* cloning into pFU189 *Not*I
3xFlagF	GGTGGTGACTACAAGGACCACGACGGCGATTATAAGGATCACGATATCGATTACAAGGACGATGACGACAAGTGAAGC	3xFlag cloning into pFU189
3xFlagR	GGCCGCTTCACTTGTCGTCATCGTCCTTGTAATCGATATCGTGATCCTTATAATCGCCGTCGTGGTCCTTGTAGTCACCACCTGCA	3xFlag cloning into pFU189
VI532	GACTGCAGATTCTGTGAGAAATC	*cnfY* aa1-719 rev *Pst*I
VI533	GACTGCAGACTGACCACCTTT	*cnfY* aa 1-526 rev *Pst*I
VI958	CGTGCAAAAACAACTGTACTCCCTGTTAAAGTACCAGAG	*cnfY* SDM C866S fwd
VI959	CTCTGGTACTTTAACAGGGAGTACAGTTGTTTTTGCACG	*cnfY* SDM C866S rev
VII006	TATCACCTGCAGGAATATTGTACTTTTCCAAAAAATC	*cnfY* 1-443 rev *Pst*I
VII006	TATCACCTGCAGGAATATTGTACTTTTCCAAAAAATC	*cnfY* 1-443 rev *Pst*I
VII061	AAGTTTAGTACAACAGATTTTTCTAATCTC	*cnfY* 39-134 deletion fwd
VII062	GAGATTAGAAAAATCTGTTGTACTAAACTT	*cnfY* 39-134 deletion rev
VII063	TATTTTTTGAGAGATAACATACTTAATAAA	*cnfY* 134-426 deletion fwd
VII064	TTTATTAAGTATGTTATCTCTCAAAAAATA	*cnfY* 134-426 deletion rev
VII065	AAGTTTAGTACAACAAACATACTTAATAAA	*cnfY* 39-426 deletion fwd
VII066	TTTATTAAGTATGTTTGTTGTACTAAACTT	*cnfY* 39-426 deletion rev
VII066	TTTATTAAGTATGTTTGTTGTACTAAACTT	*cnfY* 39-426 deletion rev
VII765	CTGAAAGGTGGTCAGAACGTAGCTGAAATT	*cnfY* 527-719 deletion fwd
VII766	AATTTCAGCTACGTTCTGACCACCTTTCAG	*cnfY* 527-719 deletion rev
VII849	CTGAAAGGTGGTCAGCCACCAGTAAAACCA	*cnfY* 527-699 deletion fwd
VII850	TGGTTTTACTGGTGGCTGACCACCTTTCAG	*cnfY* 527-699 deletion rev
VIII261	GATGAGTTAATAAACGGGGATACTTATAAAAAGCGTCGCTCTGCA	*cnfY* SDM E382/383K fwd
VIII262	TGCAGAGCGACGCTTTTTATAAGTATCCCCGTTTATTAACTCATC	*cnfY* SDM E382/383K rev
VIII263	CAGCCATTTAACTTCGAGGGGCTTGATCTTGCTGGTTATTTTATAGATAAACCATATTCTGAA	*cnfY* SDM I535L/P536A/V537G fwd
VIII264	TTCAGAATATGGTTTATCTATAAAATAACCAGCAAGATCAAGCCCCTCGAAGTTAAATGGCTG	*cnfY* SDM I535L/P536A/V537G rev
VIII265	AACTTCGAGGGGCTTGATCTTGCTGGTTATTTAATAGCTGCACCATATTCTGAACTTGCATC	*cnfY* SDM F539L/D541A/K542A fwd
VIII266	GATGCAAGTTCAGAATATGGTGCAGCTATTAAATAACCAGCAAGATCAAGCCCCTCGAAGTT	*cnfY* SDM F539L/D541A/K542A rev
FL_f_NotI	AAGAATGCGGCCGCATGAAAAATCAATGGCAACATC	*cnfY* 1-1014 forward *Not*I for cloning into modified pCOLA Duet-1
FL_r_KpnI	GGGGTACCTTAAAAGTCTTTTTGTAAAACATTAAACACAACC	*cnfY* 1-1014 reverse *Kpn*I for cloning into modified pCOLA Duet-1
526_f_NotI	AAGAATGCGGCCGCCAGCCATTTAACTTCG	*cnfY* 526-1014 forward *Not*I for cloning into modified pCOLA Duet-1
Flag3_r_KpnI	GGGGTACCTCACTTGTCGTCATCGTC	*cnfY* 526-1014 3 x Flag reverse *Kpn*I for cloning into modified pCOLADuet-1

GGS_TEM_F	GGCGGTAGCGGTGGCAGCCCAGAAACGCTGGTGAAA	Amplifcation of TEM gene, forward primer
GGS_NotI_F	AAGAATGCGGCCGCTCCGGAGGCGGTAGCGGTGGCAGC	TEM forward *Not*I primer
TEM_pVP008_R	GAGAATGGTACCTTACCAATGCTTAATCAGTG	Amplifcation of TEM gene, reverse primer
CNFy1_pVP008_NotI_F	TCCAGGGAGGCGGCCGCATGAAAAATCAATGGCAACATC	*cnfY* 1-1014 forward *Not*I for cloning into pVP008 intermediate plasmid
CNFy526_TEM_BspEI_R	CGCTACCGCCTCCGGACTGACCACCTTTCAGTCCTC	*cnfY* 1-526 reverse *BspE*1 for cloning into pVP008 intermediate plasmid
CNFy1014_TEM_BspEI_R	CGCTACCGCCTCCGGAAAAGTCTTTTTGTAAAACATT	*cnfY* 1-1014 reverse *BspE*1 for cloning into pVP008 intermediate plasmid
CNFy1_pET28a_NdeI_F	CGCGCGGCAGCCATATGATGAAAAATCAATGGCAA	*cnfY* 1-1014 forward *Nde*1 for cloning into pET28a
TEM_pET28a_HindIII_R	GTGCGGCCGCAAGCTTTTACCAATGCTTAATCAGTGAGG	TEM reverse *Hind*III for cloning into pET28a

Appendix Figures

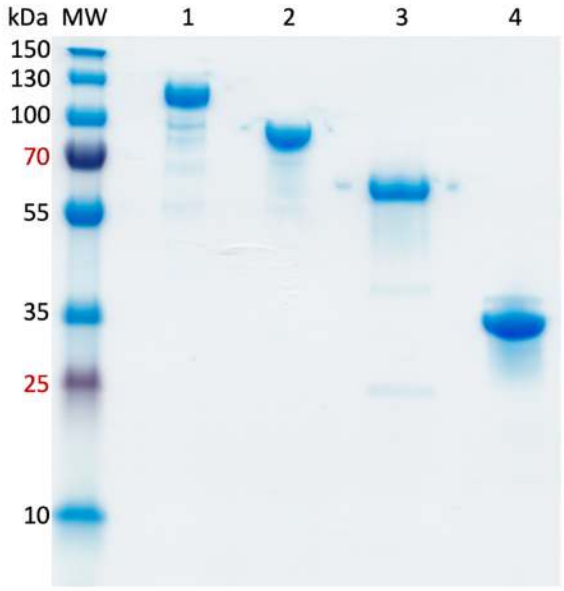

Figure S1. SDS-PAGE of purified CNF$_Y$ fragments for crystallization
Coomassie-stained SDS-PAGE (Any kD Mini-PROTEAN TGX, Bio-Rad). The fragments have been produced in *E. coli* and were purified as described in the methods section. MW: Molecular weight standard (PageRuler Plus prestained ladder, Thermo), 1: CNF$_Y$ full-length, 2: CNF$_Y$ 1-704, 3: CNF$_Y$ 526-1014, 4: CNF$_Y$ 720-1014. 2 µg of each construct have been loaded onto the gel.

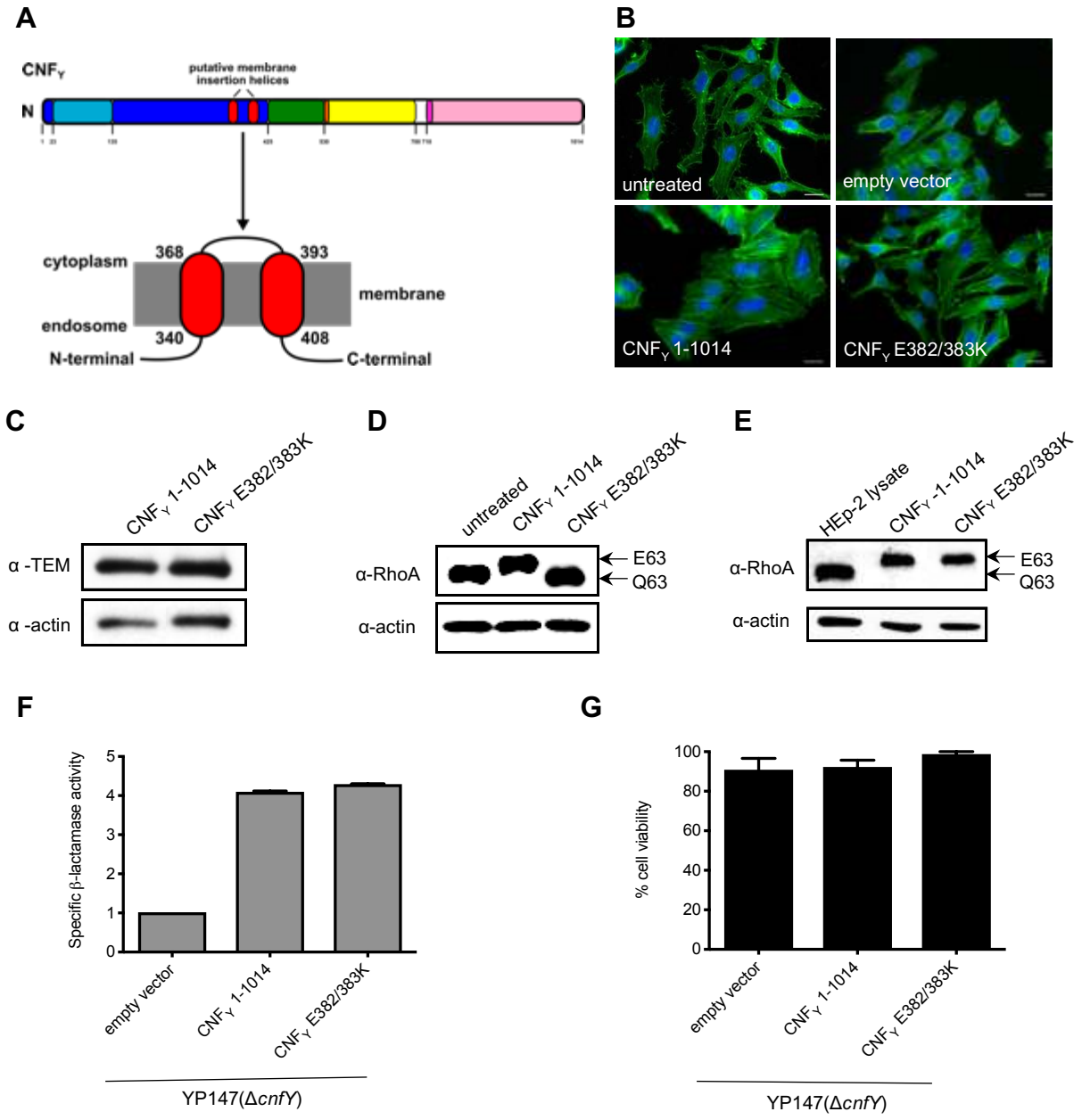

Figure S2. Characterization of secretion, cell binding, and activity of the CNF$_Y$ E382/383K variant.
A A schematic overview of CNF$_Y$ illustrating the predicted helical regions of the D2 domain exposing the acidic loop.
B HEp-2 cells were incubated with 20 µg/ml of whole cell extract of *Y. pseudotuberculosis* expressing CNF$_Y$, the toxin variant CNF$_Y$ E382/383K or no CNF$_Y$ protein (harboring empty vector) for 24 h. The formation of large, multinuclear cells was observed by fluorescence microscopy. The cell nuclei were strained with DAPI (blue) and the actin cytoskeleton was stained using FITC-Phalloidin (green). The white scale bar is 20 µm.
C The binding of CNF$_Y$ to HEp-2 cells was analyzed by immunoblotting after HEp-2 cells were incubated with 20 µg/ml of whole cell extract of *Y. pseudotuberculosis* expressing CNF$_Y$ for 4 h.
D Cells incubated with 20 µg/ml of whole cell extract of *Y. pseudotuberculosis* expressing CNF$_Y$ and the toxin variant CNF$_Y$ E382/383K for 4 h were lysed and the deamidation of RhoA was analyzed by the mobility shift of the modified GTPase detected by immunoblotting.
E The activity of the purified CNF$_Y$ derivatives was tested by analyzing the deamidation of RhoA in HEp-2 cell lysates by the mobility shift of the modified GTPase detected by immunoblotting.
F CNF$_Y$-TEM and CNF$_Y$ E382/383-TEM secretion was determined by measuring changes in absorbance of nitrocefin at 390 nm (yellow) and 486 nm (red).
G The microbial viability of the bacteria expressing CNF$_Y$ and CNF$_Y$ E382/383 was assessed in equalized bacterial cultures using the BacTiter-Glo™ Microbial Cell Viability Assay kit.

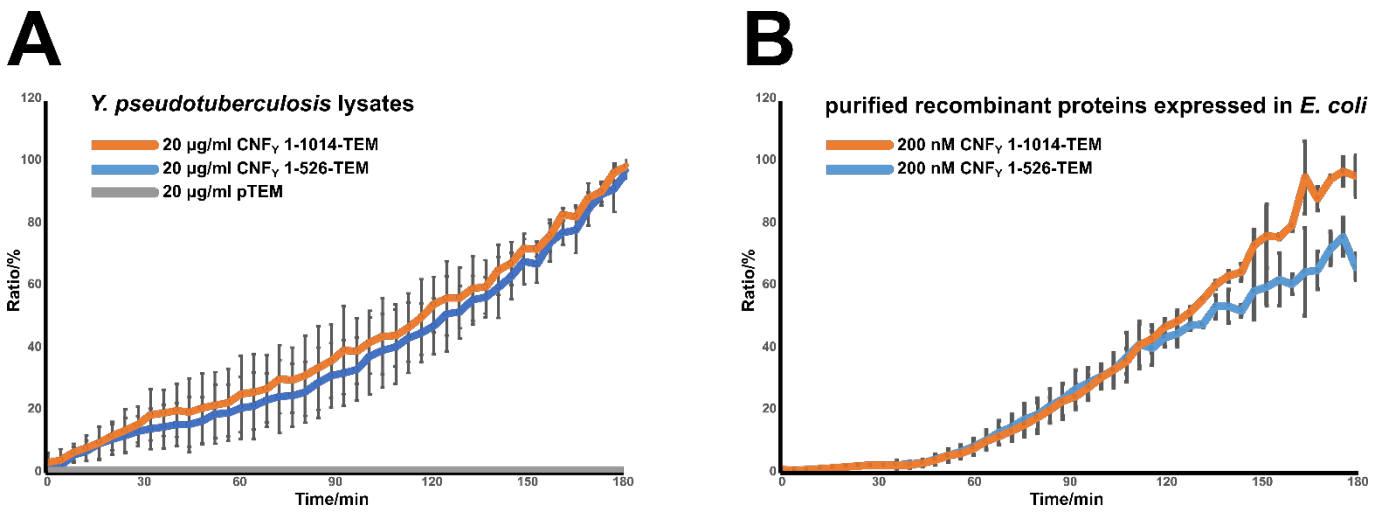

Figure S3. Translocation efficiency of full-length CNF_Y vs. CNF_Y 1-526
HEp-2 cells were loaded with CCP4-AM and then incubated with the indicated CNF_Y-TEM fusion proteins applied either as (A) lysates from *Y. pseudotuberculosis* or as (B) purified recombinant proteins purified from *E. coli*. The development of blue fluorescence, indicating translocation of TEM-β-lactamase into the cytosol, is plotted for 3 h, taking the final reading as 100%. Error bars represent standard deviations of (A) eight or (B) three replicates. Lysate from *Y. pseudotuberculosis* harboring just the pTEM plasmid served as a negative control and demonstrates that TEM-β-lactamase cannot enter HEp-2 cells when it is not fused to the translocation machinery (A).

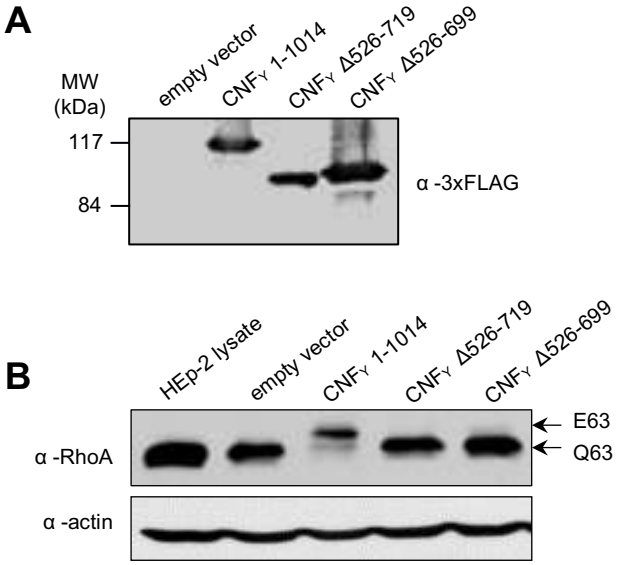

Figure S4. Expression and analysis of CNF_Y Δ527-719 or CNF_Y Δ527-699 deletion proteins missing domain D3.

A Expression of 3xFlag-lagged version of CNF_Y wildtype protein (CNF_Y1-1014 aa) and the internal deletion derivatives CNF_YΔ526-699 and CNF_YΔ526-719.

B HEp-2 cell lysates were incubated with 20 µg/ml of whole cell extract of *Y. pseudotuberculosis* expressing the indicated CNF_Y protein and their activity was tested by analyzing the deamidation of RhoA in HEp-2 cell lysates by the mobility shift of the modified GTPase detected by immunoblotting.

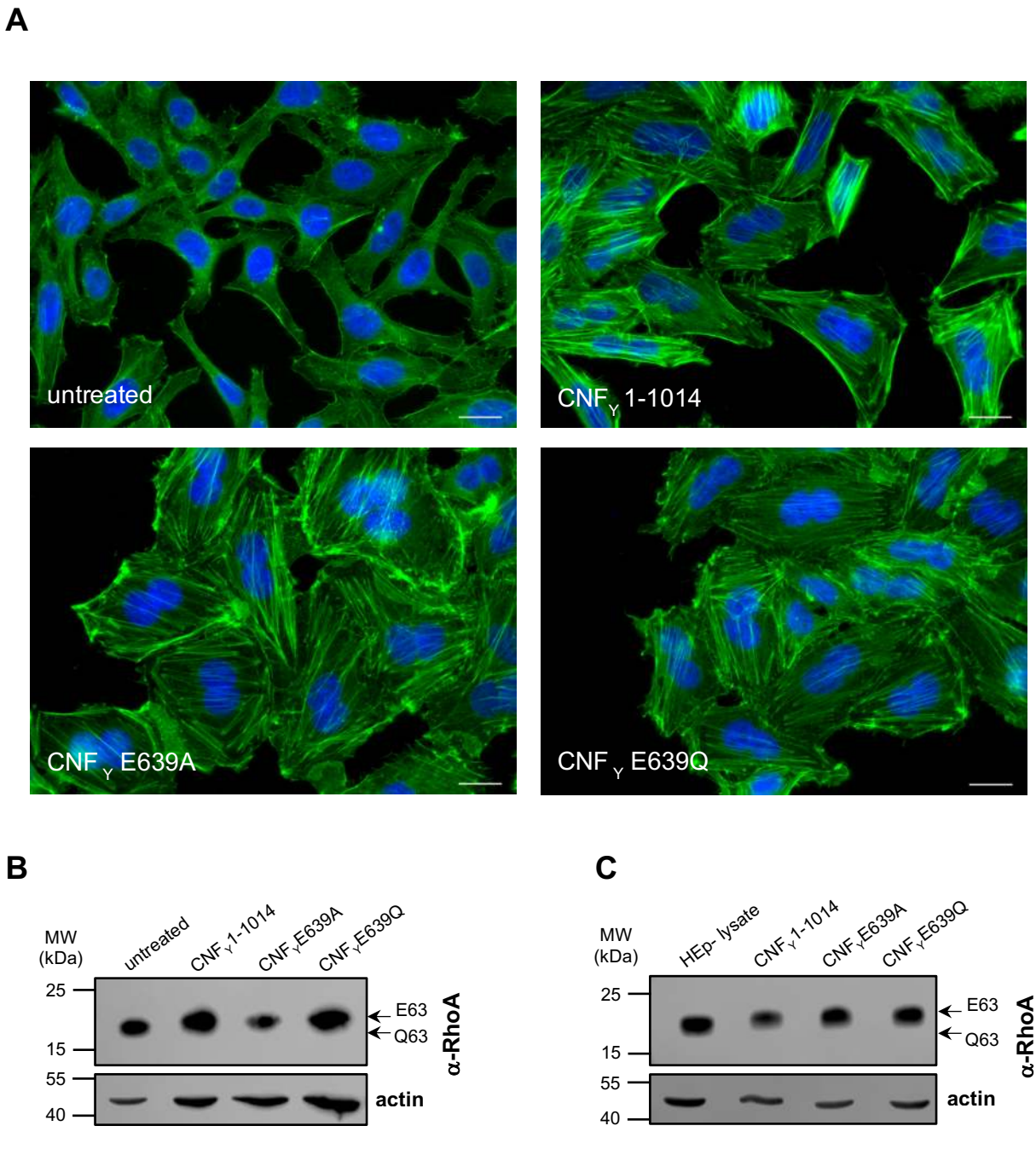

Figure S5. Expression of CNF$_Y$ E639A and 639Q and *in vitro* deamidation of RhoA.
A Purified CNF$_Y$ E639A and 639Q proteins (500 nM) were added to HEp-2 cells for 24 h. Cell nuclei were strained with DAPI (blue) and the actin cytoskeleton was stained using FITC-phalloidin (green) after treatment of cells with CNF$_Y$ toxins and cells assessed by microscopy. The white scale bar is 20 µm.
B HEp-2 cells treated with 500 nM purified full-length CNF$_Y$, CNF$_Y$ CNF$_Y$ E639A and 639Q were lysed and the deamidation of RhoA was analyzed by the mobility shift of the modified GTPase detected by immunoblotting.
C The activity of the CNF$_Y$ mutant proteins were tested by analyzing the deamidation of RhoA in HEp-2 cell lysates by the mobility shift of the modified GTPase detected by immunoblotting.

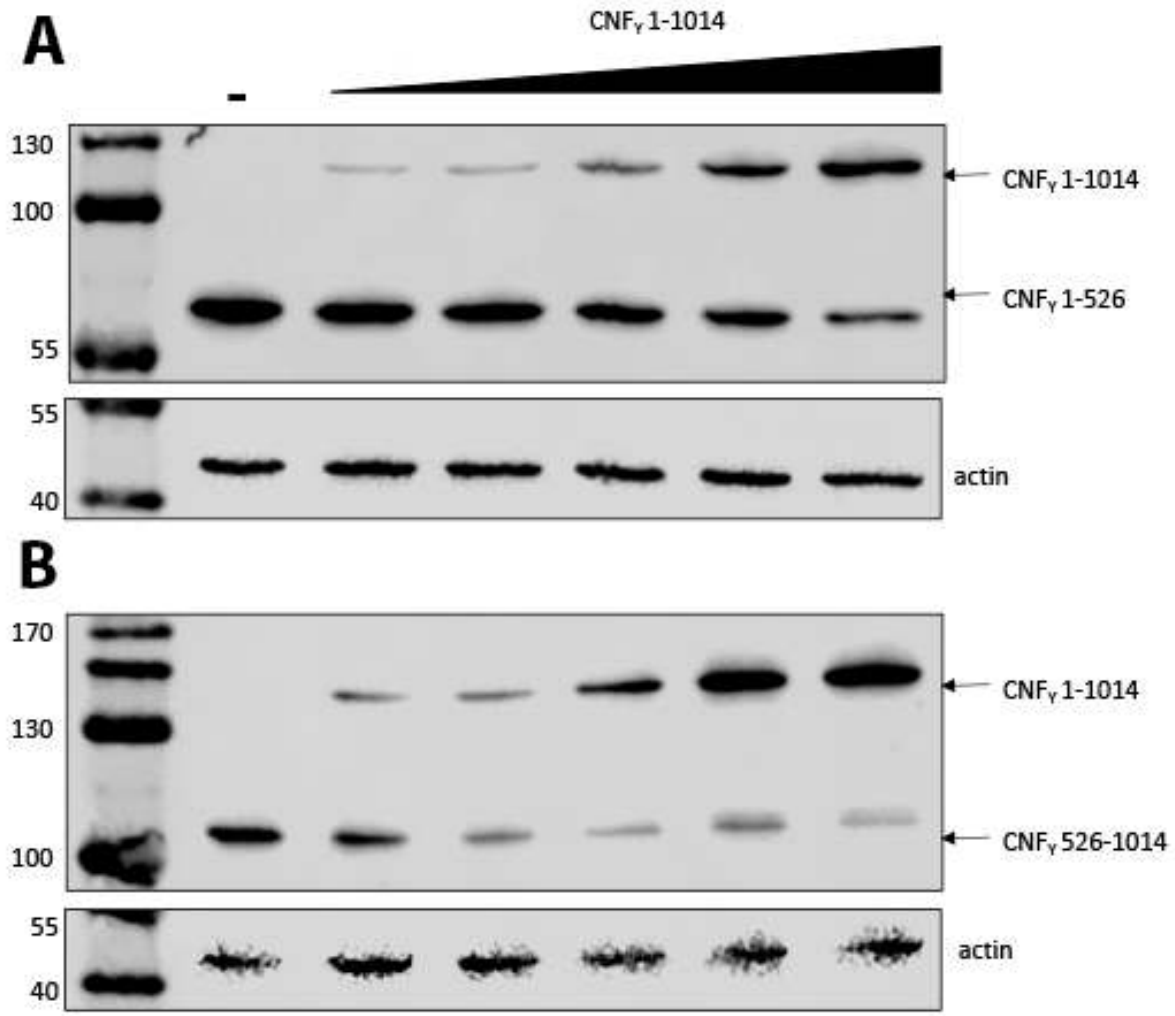

Fig. S6: **Binding of the CNF_Y D1-3 and D4-5 domain can be efficiently replaced by full-length CNF_Y.**
HEp-2 cells were incubated with 25 µg/ml of 3xFlag-tagged CNF_Y 1-526 (**A**) or CNF_Y 526-1014 (**B**) and no (-) or increasing amounts of the full-length 3x-Flag-tagged CNF_Y protein (25, 50, 100, 250, and 500 µg/ml bacterial extract of bacteria overexpressing the toxin derivatives) at 4°C for 1 h. Subsequently, whole cell extracts were prepared and bound CNF_Y proteins were detected by Western blotting using a monoclonal anti-FLAG antibody.

Appendix References

Bolin I, Norlander L, Wolf-Watz H (1982) Temperature-inducible outer membrane protein of *Yersinia pseudotuberculosis* and *Yersinia enterocolitica* is associated with the virulence plasmid. *Infect Immun* 37: 506-12.

Holm L, Rosenstrom P (2010) Dali server: conservation mapping in 3D. *Nucleic Acids Res* 38: W545-9

Karplus PA, Diederichs K (2012) Linking crystallographic model and data quality. *Science* 336: 1030-3

Krissinel E, Henrick K (2007) Inference of macromolecular assemblies from crystalline state. *Journal of molecular biology* 372: 774-97

Larkin MA, Blackshields G, Brown NP, Chenna R, McGettigan PA, McWilliam H, Valentin F, Wallace IM, Wilm A, Lopez R, Thompson JD, Gibson TJ, Higgins DG (2007) Clustal W and Clustal X version 2.0. *Bioinformatics* 23: 2947-8

Robert X, Gouet P (2014) Deciphering key features in protein structures with the new ENDscript server. *Nucleic Acids Research*, 42: W320–W324.

Schweer J, Kulkarni D, Kochut A, Pezoldt J, Pisano F, Pils MC, Genth H, Huehn J, Dersch P (2013) The cytotoxic necrotizing factor of *Yersinia pseudotuberculosis* (CNF_Y) enhances inflammation and Yop delivery during infection by activation of Rho GTPases. *PLoS Pathogens* 9: e1003746

Uliczka F, Dersch P (2012) Unique virulence properties of *Yersinia enterocolitica* O:3. *Adv Exp Med Biol* 954: 281-7